materials

MDPI

Review

CO_2 Hydrogenation to Methanol over Metal–Organic Framework Catalysts: Reaction Pathways and Catalyst Design Strategies

Abdul Malik P. Peedikakkal [1,2]

[1] Department of Chemistry, King Fahd University of Petroleum & Minerals, Dhahran 31261, Saudi Arabia; abdulmalik@kfupm.edu.sa
[2] Center for Refining and Advanced Chemicals, King Fahd University of Petroleum & Minerals, Dhahran 31261, Saudi Arabia

Abstract

Conversion of CO_2 into fuels and value-added chemicals is an emerging area that enables the evolution toward a circular carbon economy. CO_2 can be utilized to produce methanol, ethanol, methane and light olefins through renewable hydrogen. Metal–organic frameworks (MOFs) are an excellent platform for thermocatalytic CO_2 hydrogenation to methanol, as their metal nodes, organic linkers, defects and confined pore environments can be engineered to enhance CO_2 adsorption, H_2 activation and stabilization of crucial reaction intermediates. However, many MOFs still suffer from drawbacks such as low thermal stability, limited mass transport, weak metal-support interaction and potential framework destruction under hydrogenation conditions, which can limit methanol productivity and long-term catalyst stability. This review summarizes recent progress in MOF-based catalysts and MOF-derived materials for CO_2 hydrogenation to methanol, with a focus on reaction pathways, pore confinement, active-site design, catalyst stability, and structure-performance relationships. The advantages and remaining limitations of MOF systems are discussed in comparison with conventional heterogeneous catalysts, and future strategies are proposed for developing more selective, durable, and energy-efficient catalysts for sustainable methanol synthesis.

Keywords: metal–organic framework; carbon dioxide; CO_2 conversion; methanol synthesis; hydrogenation

1. Introduction

During the last century, carbon dioxide (CO_2) has become one of the most important greenhouse gases, contributing to anthropogenic climate change [1,2]. CO_2 levels are rising in the atmosphere, which has increased concerns about global warming and environmental damage. CO_2 is abundant in the atmosphere, which can be converted into useful chemicals and fuels through catalytic processes, which creates valuable products [3]. Although, CO_2 valorization alone cannot resolve concerns over rising atmospheric CO_2 levels. The conversion of CO_2 into hydrocarbons and oxygen-containing compounds has received significant attention in recent years. There are many studies showing that these conversions can be achieved not only in the laboratory but also on a pilot scale. Due to its wide availability, CO_2 is particularly appealing from an industrial standpoint, with annual global emissions estimated at 3300–3500 million tons [4]. However, its high thermodynamic stability, coupled with its chemical inertness, makes it particularly challenging to activate and convert CO_2 [5]. Although CO_2 is chemically inert, fuels and chemicals can still be made using CO_2 as a C_1

Check for updates

Academic Editor: Zhen Xu

Received: 19 September 2026
Revised: 10 November 2026
Accepted: 19 November 2026
Published: 27 November 2026

Copyright: © 2026 by the author. Licensee MDPI, Basel, Switzerland. This article is an open access article distributed under the terms and conditions of the Creative Commons Attribution (CC BY) license.

source. Catalytically transforming CO_2 into valuable products in a sustainable way at least allows for emissions to be mitigated whilst creating a more circular carbon economy [6–9]. Different strategies have been explored to convert CO_2. These include electrochemical, photocatalytic, and thermocatalytic approaches. Electrochemical and photocatalytic routes have been emphasized frequently since renewable electricity or sunlight can be used as energy sources for carbon dioxide reduction reaction (CO_2RR). With the continual improvement of catalyst activity, such processes can be conducted at milder conditions, which can reduce energy consumption [10–12]. However, applying electro- and photocatalytic methods in practice is often limited by electricity supply and light availability, which can affect their economic viability. By contrast, thermocatalytic CO_2 conversion tends to be more efficient and better suited for large-scale industrial use. Due to the thermodynamic stability and chemical inertness of CO_2, a substantial energy input is needed for the activation of the C=O bond. In this context, renewable H_2 with high gravimetric energy density produced via water electrolysis or photolysis has been employed as a reductant widely. Accordingly, CO_2 conversion into value-added products such as methane (CH_4), methanol (CH_3OH), ethanol (C_2H_5OH), and light olefins (C_2–C_4) has received growing interest [13].

The conversion of CO_2 into methanol through hydrogenation has gained a lot of interest because of methanol's versatility. It can serve as a fuel, a hydrogen carrier, and act as an intermediate building block in the chemical industry. Another advantage is that methanol could be easily integrated into the current industry systems. That is why it is often seen as an important part of the growing methanol-based economy. But the efficiency of the whole process is very much determined by the catalyst design. The nature of active sites, metal-support interactions, and stability of reaction intermediates are examples of such parameters. In this context, catalyst supports are crucial. They help improve performance by providing a large surface area, promoting better metal distribution, and affecting the electronic and structural features of the active sites [14]. In recent years, metal–organic frameworks (MOFs) have attracted attention as promising materials for adsorption, gas separation, and catalysis. This interest stems mainly from their high surface areas, the many metal active sites, and their well-organized three-dimensional porous networks [15,16]. Metal–organic frameworks (MOFs) are made from either metal ions or metal clusters, in which the metal clusters can act as secondary building units (SBUs). These metal ions or metal clusters connect through organic ligands to form extended network structures [17,18]. The internal pores, unsaturated metal sites created via the removal of coordinated solvents and structural flaws in MOFs, such as missing linkers, create active site for catalytic conversion. The pores can be also utilized to stabilize tiny metal nanoparticles. This confined space restricts particle growth and stops them from sticking together. This helps keep active sites during catalytic processes [19–23]. Furthermore, the interaction between metal species and the support structure can be modulated by precise control of the heat treatment process applied to MOF materials, particularly the pyrolysis of coordinated organic molecules [21,24,25].

Several recent reviews have discussed the development of catalysts and reaction strategies for CO_2 conversion and hydrogenation. Pan et al. reviewed heterogeneous catalysts for CO_2 hydrogenation to methanol, including the thermodynamic and kinetic aspects of the reaction, the direct CO_2 to methanol and reverse water-gas shift pathways, the influence of temperature, pressure, the H_2/CO_2 ratio and water, and the development of supported metal, oxide and alloy catalysts [26]. Wen et al. reviewed carbon-based catalysts for thermocatalytic CO_2 hydrogenation toward a circular economy, covering porous carbon, carbon nanotubes, graphene and MOF-derived carbon materials. Their analysis emphasized the roles of carbon-support properties, metal dispersion, carbon–metal interactions, catalytic activity and product selectivity [27]. Liao et al. further reviewed carbon-material-driven photothermal CO_2 reduction, focusing on the synergistic effects of light and heat, photother-

mal reaction mechanisms, carbon-based active and regulatory phases, interface engineering, heteroatom doping, structural modification and the techno-economic and environmental aspects of photothermal CO_2 conversion [28].

These studies have significantly advanced the understanding of CO_2 conversion and methanol synthesis. However, they mainly discuss heterogeneous catalysts in general, carbon-based systems, MOF-derived carbon materials or photothermal CO_2 reduction. The specific role of MOF architectures in thermocatalytic CO_2 hydrogenation to methanol requires further focused analysis. In particular, the effects of MOF metal nodes, organic linkers, framework defects, pore size, pore polarity, nanoparticle confinement, metal–support interactions and MOF-derived phases should be considered in relation to CO_2 adsorption, H_2 activation, reaction-intermediate stabilization, methanol selectivity, product diffusion and catalyst stability. Therefore, the present review focuses specifically on MOF-based and MOF-derived catalysts for thermocatalytic CO_2 hydrogenation to methanol and connects the framework structure with the reaction pathway, active-site environment and catalytic performance.

Unlike general reviews on methanol synthesis or broad MOF catalysis, this review focuses specifically on how MOF structure controls performance in CO_2 hydrogenation to methanol. Particular attention is given to structure-performance relationships, such as pore confinement, defect engineering, linker functionalization, metal-node chemistry, nanoparticle encapsulation, and metal-support interactions. In addition, the review correlates these structural motifs to the formate and the redox water gas shift (RWGS)-based reaction mechanisms, catalyst stability, and the technological hurdles that should be overcome for MOF-derived catalysts to be envisioned in large-scale methanol production. Accordingly, this review focuses on the reaction pathways of CO_2 hydrogenation to methanol, the role of MOF pore confinement, active-site and catalyst design, catalyst stability, and the relationship between MOF structure and catalytic performance.

2. Fundamentals of CO_2 Hydrogenation to Methanol

2.1. CO_2 Properties

Carbon dioxide (CO_2) is a linear molecule consisting of a single carbon atom that has two oxygen atoms bonded to the atom by a double bond [29]. These C=O bonds are very strong, and this renders CO_2 very stable. Its bond length is approximately 116.3 pm (1.163 Å), and the bond energies are approximately 799 kJ mol^{-1} and the dissociation energy of the bond is approximately 531.7 kJ mol^{-1} s [29]. Carbon is already in the most oxidized form in CO_2, the molecule is already a final product of oxidation and cannot easily react, so its activation is difficult. With regard to the distribution of electrons, the bulk of the electron density is found around the oxygen atoms, which leaves the carbon atom comparatively electron-poor and highly electrophilic. This implies that the carbon center is able to react with electron-rich species like bases or electron-giving ligands. To excite CO_2, catalysts are normally employed to drive the electron density into its antibonding orbitals that loosen the C=O bonds, enabling other reactions such as hydrogenation or carbon-carbon coupling to take place. More specifically, electron-donating ligand-based homogeneous catalysts have been demonstrated with high performance, and, therefore, transition metal complexes are very common in the CO_2 conversion processes [29,30]. The key physicochemical properties of CO_2 relevant to its catalytic activation are summarized in Table 1.

Table 1. General characteristics of CO_2 molecules [31,32].

Species	Phase Transition Temperature (°C)	Bond Polarity	ΔH_f (298 K) (kJ mol^{-1})	Bond Energy (kJ mol^{-1})	C–O Bond Length (Å)	Geometry	Bond Angle (°)	Partial Charges
CO_2	−78.5 (sublimation)	1.0	−393.5	806	1.169	Linear	180	C: +0.719; O: −0.360

2.2. Thermodynamics of CO_2 Hydrogenation

The hydrogenation of CO_2 to methanol is thermodynamically challenging because CO_2 is highly stable, as reflected by its large negative standard enthalpy of formation. Therefore, high-energy co-reactants are required to drive its conversion [33]. Among possible co-reactants, H_2 is particularly attractive because it can be produced from renewable sources, while methanol is an important chemical feedstock and energy carrier [34–36]. The major reactions involved in CO_2 hydrogenation, including methanol synthesis, the reverse water-gas shift reaction, and methanation, are summarized in Table 2 [37].

Among these pathways, methanation is thermodynamically more favorable than methanol synthesis because of its highly negative Gibbs free energy and large equilibrium constant. As a result, methane formation can become significant, especially at elevated temperatures or over catalysts with strong hydrogenation activity. In contrast, methanol synthesis is exothermic but equilibrium-limited, while the RWGS reaction is endothermic and competes with methanol formation by producing CO and water [38–40]. Therefore, catalyst design must suppress over-hydrogenation to methane and stabilize key intermediates involved in methanol formation.

Reaction conditions also strongly influence methanol yield and selectivity. Lower temperatures thermodynamically favor methanol formation and help suppress RWGS, but they may reduce reaction rates. Higher pressures favor methanol synthesis because the reaction proceeds with a decrease in the total number of gas-phase molecules. The H_2/CO_2 ratio also affects both equilibrium and reaction kinetics [38]. In general, Cu- and Ag-based catalysts tend to favor methanol formation, whereas Ni- and Ru-based catalysts promote methanation; Pd-, Pt-, Rh-, Mo-, and Au-based systems often produce mixtures of methanol and methane [41].

Thermodynamic calculations, often carried out by use of FactSage, are useful for evaluating equilibrium CO_2 conversion and product distribution at the actual reaction conditions of 170–300 °C, 1–50 bar, and an H_2/CO_2 ratio of 3:1 [42,43]. In general, a high activity combined with a high methanol selectivity is needed to realize an efficient conversion of CO_2 to methanol, which can only be obtained by a fine balancing of temperature, pressure, feed composition and catalyst structure.

Table 2. Thermodynamic parameters of key reactions in CO_2 hydrogenation to methanol [44].

Entry	Reaction	$\Delta G°$ (kJ mol^{-1})	$\Delta H°$ (kJ mol^{-1})	K°
1	$CO_2 + 4H_2 \rightarrow CH_4 + 2H_2O$	−113.5	−165.0	7.79×10^{19}
2	$CO_2 + H_2 \rightarrow CO + H_2O$	28.6	41.2	9.67×10^{-6}
3	$CO_2 + 3H_2 \rightarrow CH_3OH + H_2O$	3.5	−49.3	2.45×10^{-1}

2.3. CO_2 Hydrogenation to Methanol Reaction Mechanism

Rational design of active and selective CO_2 to methanol catalysts requires a clear understanding of the reaction pathways by which CO_2 is transformed into methanol [45]. Two broad mechanisms are usually considered, as shown in Figure 1. In the CO-mediated route, CO_2 is first converted to surface CO species through direct C=O bond cleavage or

carboxyl-type intermediates; adsorbed CO is then hydrogenated stepwise to methanol. In the formate route, adsorbed CO_2 is hydrogenated to surface formate (HCOO*) species, which are further reduced through successive hydrogenation steps to methanol. The preferred pathway depends on how the catalyst stabilizes COOH*, HCOO*, CO*, methoxy, and related intermediates. For example, Cu/ZnO-based catalysts generally favor the formate route, whereas Cu/CeO_2, Cu/TiO_2, and Cu/ZrO_2 systems may follow a CO-mediated mechanism when formate species are too strongly adsorbed and inhibit further hydrogenation [46]. Promoters and support modifications can tune intermediate binding strengths, lower kinetic barriers, and direct the reaction toward methanol rather than CO or CH_4 [47].

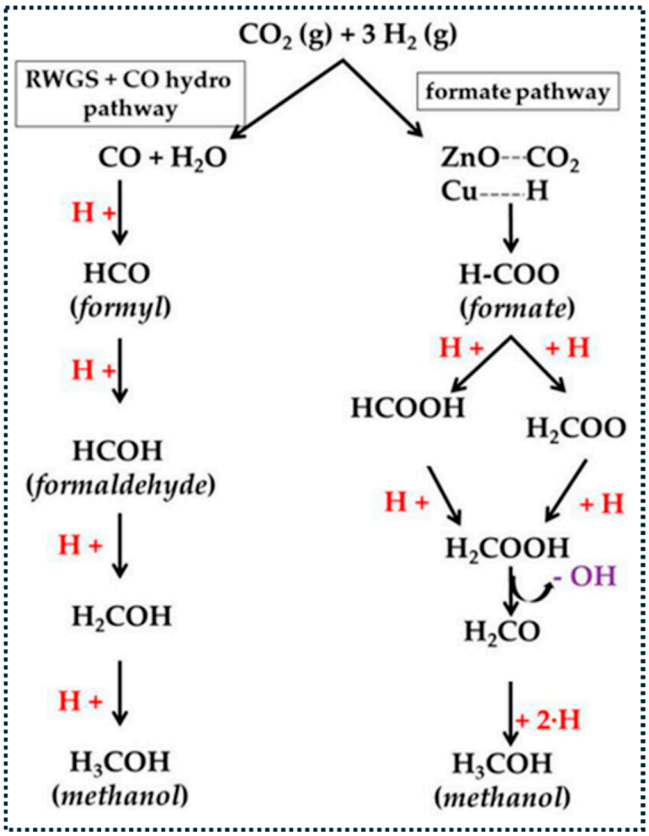

Figure 1. Schematic representation of CO_2 hydrogenation pathways leading to CH_3OH [48].

For MOF catalysts, the dominant pathway depends not only on the active metal but also the MOF node, linker environment, defect density, and pore confinement. Lewis acidic Zr-oxo nodes in UiO-type frameworks stabilize formate intermediates at metal-MOF interfaces, whereas defects and missing linkers introduce unsaturated sites that promote CO_2 adsorption and H_2 activation. In contrast, metals that strongly activate CO, like Pd- or Pt-based catalysts, possibly need to be alloyed or subjected to interfacial engineering to inhibit RWGS and CO-poisoning. Thus, reaction pathways over MOF-based catalysts are controlled by a combination of metal identity, metal-node contact, confinement, hydrophobicity/hydrophilicity, and the adsorption strength of key intermediates [19].

3. Catalytic Routes for CO_2 Hydrogenation to Methanol

CO_2 hydrogenation to methanol can be achieved through three main catalytic routes: electrocatalysis [49,50], photocatalysis [51], and thermocatalysis [52,53]. Among these, thermocatalysis remains the most mature and industrially relevant approach, while electrochemical and photocatalytic methods are mainly explored as lower-temperature routes

driven by renewable electricity or solar energy. Since this review focuses on MOF-based catalysts for methanol synthesis, the electrochemical and photocatalytic routes are introduced only briefly, with emphasis on their relevance to MOF materials, while thermocatalytic CO_2 hydrogenation is discussed in greater detail.

3.1. Electrochemical Reduction of CO_2

Electrochemical CO_2 reduction (ECR) enables the conversion of CO_2 into fuels and value-added chemicals under relatively mild conditions. It can operate near ambient temperature and pressure, making it attractive for coupling with renewable electricity and for storing electrical energy in chemical products such as methanol [54,55]. The increasing availability of renewable power sources has further strengthened interest in this approach [56]. In ECR, CO_2 is first adsorbed on the electrocatalyst surface and then activated to form reactive intermediates such as $CO_2^{\bullet-}$. Subsequent proton-coupled electron-transfer steps lead to C-O bond cleavage, C-H bond formation, and finally product desorption [57,58]. However, methanol formation competes with other CO_2 reduction products and with the hydrogen evolution reaction, which often limits selectivity [59]. Despite the mild conditions for operation and good process control in electrocatalysis, difficulties are still encountered in enhancing the methanol selectivity, inhibiting side reactions, and lowering the cost in product separation.

The relevance of MOF-based electrocatalysts relies on the fact that their metal nodes, functionalized linkers, and confined pores can enhance CO_2 adsorption, provide isolated metal sites, and adjust the local proton/electron environment. Nevertheless, controlling the selectivity for methanol is still a challenge, as the overall performance is significantly affected by multi-electron transfer, HER competition, electrolyte effects, and product separation. In other words, ECR is considered here as a successful example of the complementary low-temperature approach, not as the main approach discussed in this review.

3.2. Photocatalytic Reduction of CO_2

Photocatalytic CO_2 reduction relies on light absorption to produce electron-hole pairs that participate in surface redox reactions [60,61]. In principle, this route can use solar energy to convert CO_2 and H_2 into products such as CH_4, CO, formic acid, and methanol. MOFs can contribute by incorporating photoactive linkers, catalytic metal nodes, or guest nanoparticles within ordered pores, thereby improving CO_2 uptake and spatial organization of active sites.

The main limitations are rapid charge recombination, insufficient visible-light absorption, low quantum efficiency, and competing reduction products [62–67]. For methanol synthesis, the problem is particularly acute as multiple coupled electron/proton transfers are involved. Hence, MOF-based photocatalytic systems are still intriguing but inferior to thermocatalytic systems in the large-scale practical production of methanol.

3.3. Thermocatalytic Heterogeneous Reduction of CO_2 to Methanol

Thermocatalytic CO_2 hydrogenation is the most mature route to methanol production, since it is compatible with fixed-bed reactor technology and assumes that renewable H_2 will be produced by water electrolysis [68]. The main reactions are direct CO_2 hydrogenation to methanol, RWGS and hydrogenation of the produced CO, as shown in Table 3. Conventional heterogeneous catalysts, such as Cu-based oxides, depend upon metal-oxide interfaces that enable activation of CO_2 and H_2 and dictate product selectivity [69–73]. MOF-based thermocatalysts extend this principle by exploiting ordered pores, Lewis acidic nodes, defects, and confinement to disperse metal nanoparticles, to produce well-defined interfacial sites, and to stabilize methanol-forming intermediates. Yet, high temperature and pressure

may still be required, and the stability of MOFs, or MOF-derived materials, under water-rich reaction conditions remains a central challenge.

Table 3. Key reaction pathways involved in CO_2 conversion to methanol.

Equation No.	Reaction Equation	Process Type	Notes
1	$CO_2 + 3H_2 \rightarrow CH_3OH + H_2O$	Direct hydrogenation	$\Delta H_{298} = -49.3$ kJ mol^{-1}, 5–10 MPa
2	$CO_2 + H_2 \rightarrow CO + H_2O$	RWGS reaction	$\Delta H_{298} = 41.2$ kJ mol^{-1}, 5–10 MPa
3	$CO + 2H_2 \rightarrow CH_3OH$	CO hydrogenation	$\Delta H_{298} = -90.7$ kJ mol^{-1}, 5–10 MPa
4	$2CH_3OH \rightarrow CH_3OCH_3 + H_2O$	Methanol dehydration	Side reaction
5	$CH_3OH \rightarrow CO + 2H_2$	Methanol decomposition	Reverse reaction

3.4. Comparison of Different Catalytic Technologies

Table 4 is a summary that compares the aforementioned catalytic strategies, revealing their principles as well as advantages and disadvantages in the conversion of CO_2 to methanol. In general, electrochemical and photocatalytic processes provide mild reaction conditions; however, they tend to exhibit low methanol selectivity with HER or charge recombination and product-separation problems. Thermocatalysis is still the most feasible method for CO_2-to-methanol production, yet its energy consumption and catalyst poisoning drive the design of MOF-derived materials that can function selectively at lower temperature and pressure.

Table 4. Comparison of various catalytic strategies for the hydrogenation of CO_2 to methanol.

Technique	Working Mechanism	Advantages	Limitations	Ref.
Thermal catalysis	Utilizes catalysts to lower activation energy, enabling chemical reactions to proceed more efficiently and improving reaction rates and selectivity under elevated temperatures	High efficiency; good selectivity; rapid reaction kinetics; well-established and industrially mature technology	Requires high temperature and pressure; significant energy demand; catalyst deactivation over time	[68,74]
Photocatalysis	Light irradiation excites electrons on the catalyst surface, generating electron–hole pairs that participate in redox reactions with surrounding species	Operates under mild conditions; environmentally sustainable	Low overall conversion efficiency	[75,76]
Electrocatalysis	Application of an external potential drives electron transfer between electrodes and reactants in solution, initiating chemical transformations	Simple system design; easy operation	High energy consumption; low current efficiency	[59]

4. Structural Features and Design Flexibility of MOFs

4.1. Role of MOF-Based Supports for CO_2 Conversion to Methanol

In heterogeneous catalysis, the supports affect the dispersion, stability, electronic structure, and accessibility of active metal sites. Oxides, porous carbon materials, PCN-type porous materials, molecular sieves, and zeolites can enhance dispersion and thermal stability, but their pore environments and distributions of active sites typically are less synthetically programmable than those of MOFs. MOFs offer additional advantages because

their metal nodes, organic linkers, pore size, polarity, defect density, and hydrophobicity can be tuned at the molecular level. These features allow MOFs to confine nanoparticles, stabilize ultrasmall clusters or single sites, promote uniform metal-support interfaces, and regulate CO_2 adsorption and intermediate diffusion [59,77–80]. However, MOFs also have limitations, especially framework stability and scalability under high-temperature, high-pressure, and water-forming reaction environments. Figure 2 summarizes the general functions of catalyst supports.

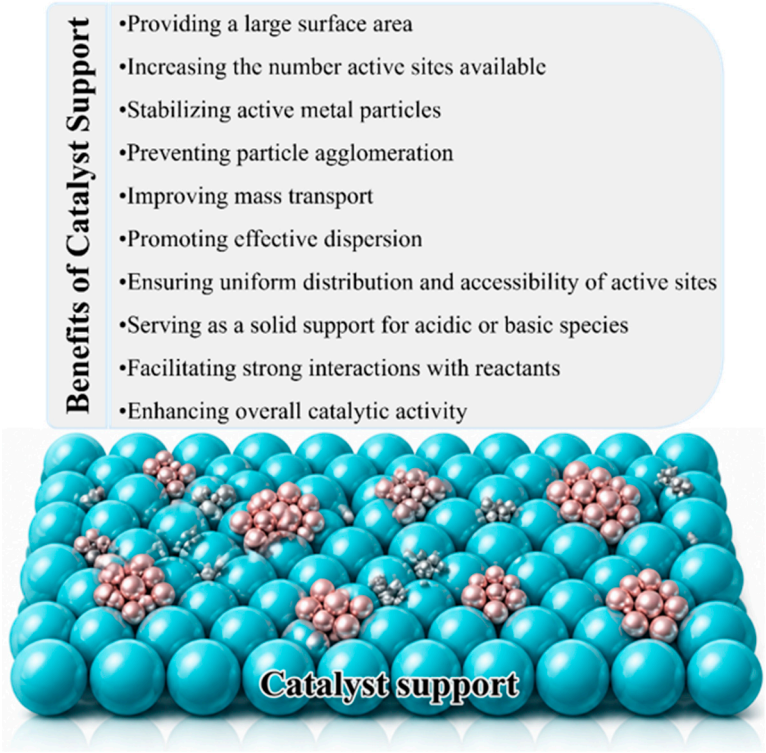

Figure 2. The role of the support in catalyst performance improvement (The support image was generated using ChatGPT 5.6, while the arrangement and other figure elements were obtained using standard software tools.).

Ordered porous solids, including zeolites and zeolite-derived carbons, are widely used as catalysts or catalyst supports because their pore networks provide accessible active sites, controlled molecular diffusion, and shape-selective reaction environments. MOFs are constructed from metal clusters joined by organic linkers to form highly porous crystalline structures (Figure 3) [79,80]. This architecture provides exceptionally high surface areas, tunable pore structures, and accessible inorganic building units. Early benchmark MOFs include MOF-2 [81] and MOF-5 [82], HKUST-1 [83], followed by MIL-101 [84], and the MOF-74 family. The properties of MOFs, like stability, surface area, and CO_2 capture properties have been reviewed in detail by Trickett et al. [85].

Several MOFs possess rigid frameworks that generate large internal voids and very high porosity. For example, NU-110E, constructed using an acetylene-expanded hexatopic linker, showed an experimentally observed BET surface area value of approximately 7100 m^2/g [85]. Later, Kaskel and co-workers synthesized DUT-60 with a surface area approaching 7800 m^2/g, among the highest values reported for porous MOFs [86]. However, such extremely high surface areas should be interpreted carefully because conventional porosity measurements may have limitations for ultraporous materials. To date, approximately more than 70,000 MOF structures have been reported [87]. Their tunable properties

have encouraged broad investigation in catalysis, adsorption, and separation, although industrial implementation remains limited [88,89].

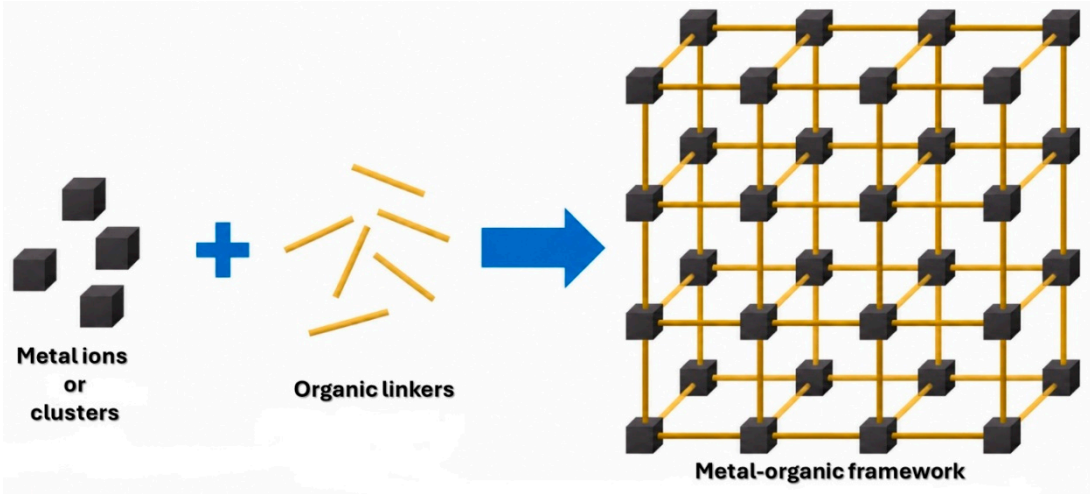

Figure 3. Schematic structure of metal–organic frameworks.

MOFs are commonly prepared through reticular synthesis, where metal-based inorganic units are connected with multitopic organic ligands through strong coordination bonds. By selecting suitable metal nodes, linkers, and synthetic conditions, MOFs can be synthesized in a controlled manner to exhibit specific pore architectures, multifunctionalities, and defect structures [87]. Further tuning is possible via pre-synthetic and post-synthetic modification to produce customized catalytic materials [90]. Although these materials are remarkably versatile, the transition of MOFs to practical catalytic applications at a large scale remains more challenging than that of zeolites, predominantly because of stability issues, scale-up, and running under severe reacting conditions [91].

In the case of CO_2 hydrogenation to methanol, the intrinsic chemical stability of CO_2 requires catalysts that can be used at high temperature and H_2 pressure. Thermally stable MOFs with high CO_2 adsorption, a tailorable pore environment, and available metal sites can be fascinating, although for this reaction they are less investigated. One of the main advantages of MOFs is that their framework structure and crystallinity are often retained when the organic linkers and/or inorganic subunits are systematically altered. Eddaoudi et al. exemplified this design versatility through the synthesis of 23 MOFs with predictable pore sizes, shapes, nanocrystal sizes, and architectural features [92]. In similar MOF series, pore diameters were modified from 8.4 to 23.9 Å with an increasing linker size [93]. These examples demonstrate that MOFs can serve as a general platform for designing catalysts with size and functionality control, but stability and scalability are still to be desired.

In recent years, several review articles have examined MOFs and their wide range of applications. These studies have discussed the historical development of MOFs, their classification and terminology, common synthesis routes, and the key parameters that influence their formation. Figure 4 shows various synthetic methods used for MOF synthesis and compares the main advantages and limitations of each approach.

4.2. Classification and Structural Families of MOFs

Depending on their structural arrangement, chemical composition, functionality, and target application, MOFs can be classified in several ways [94–96]. One widely used approach is classification on the basis of their compositional building units and framework families.

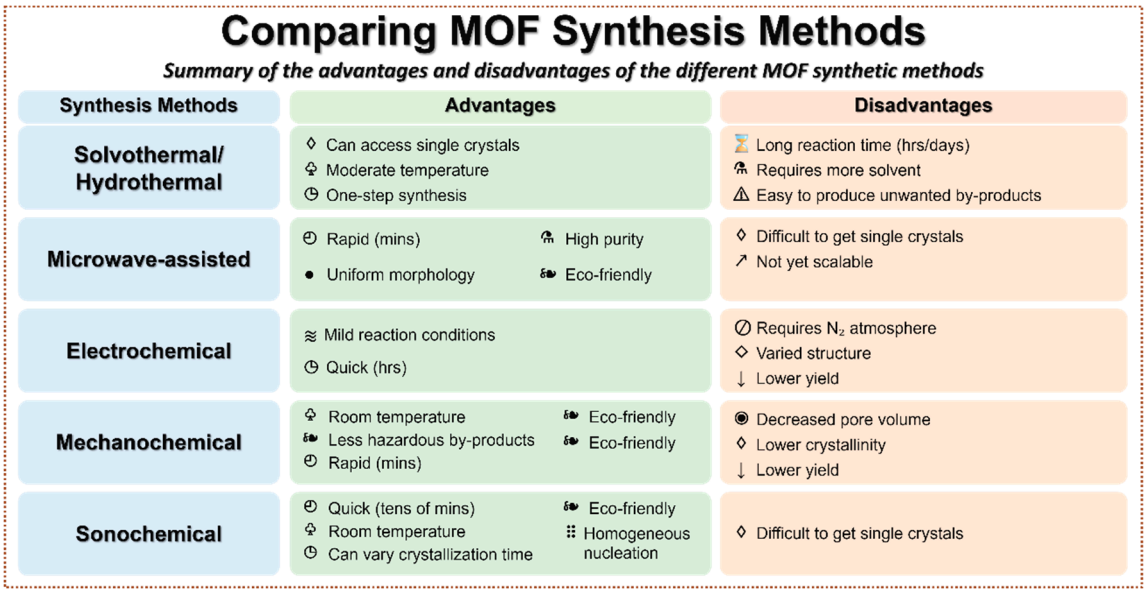

Figure 4. Comparison of the advantages and disadvantages of various MOF synthesis methods.

4.2.1. Zeolitic Imidazolate Frameworks (ZIFs)

ZIFs are an important subclass of MOFs that possess topologies like zeolite and are constructed from imidazole-based linkers. Common instances include ZIF-67, ZIF-90, ZIF-7 and ZIF-8. Out of them, ZIF-8 has received considerable attention because of its well-developed pore structure, responsiveness to environmental conditions and high surface area [97]. ZIF-based materials have been employed in CO_2 reduction, including through strategies such as introducing isolated metal atoms into the framework [98]. Owing to their excellent chemical and thermal stability, ZIFs are widely employed as robust platforms for the preparation of composite materials [99,100]. They have also been used as precursor materials for the development of catalysts applied in thermocatalytic CO_2 conversion processes [101–105], because their metal nodes and imidazolate linkers can be transformed by pyrolysis or calcination into metal/metal-oxide nanoparticles embedded in N-doped porous carbon, giving high dispersion, improved metal–support interaction, better CO_2 adsorption, and resistance to sintering during reactions such as CO_2 hydrogenation to methanol, methane, CO, hydrocarbons, and light olefins.

4.2.2. Materials Institute Lavoisier (MIL) MOFs

MIL MOFs, typically formed by connecting metal centers with carboxylate-based organic linkers, produce durable porous frameworks. Examples include MIL-125, MIL101, MIL100 and MIL88 which exhibit tunable pore structures and, in certain instances, stimuli-responsive behavior. Their ordered porosity, high surface area and structural flexibility have made MIL-based materials attractive for sensing and catalytic applications [68]. Among the various MOF-derived catalysts, materials based on MIL frameworks have demonstrated considerable potential for the thermocatalytic conversion of CO_2 to methanol [106,107].

4.2.3. Isoreticular MOFs

Isoreticular MOFs, commonly referred to as IRMOFs, constitute a well-known class of MOFs typically formed by linking $[Zn_4O]^{6+}$ SBUs with aromatic carboxylate ligands. This arrangement produces highly ordered porous frameworks with adjustable pore dimensions and chemical environments. Their structural tunability has enabled applications in thermocatalytic CO_2 conversion to methanol [108–111]. Recent theoretical studies have also provided useful guidance for the rational design of IRMOF-based materials [112].

4.2.4. Porous Coordination Polymers

MOFs are also named as porous coordination polymers (PCPs) and both term often used interchangeably. Several PCPs have been reported and their porous structures expose catalytically active sites and allow the local coordination environment around the metal centers to be tailored, making them attractive materials for a wide range of catalytic applications. Owing to these features, PCPs have been investigated for catalysis and thermocatalytic CO_2 conversion to methanol [108,113,114].

4.2.5. Porous Coordination Networks

MOFs are also named as porous coordination networks (PCNs). Several such PCNs materials characterized by high porosity and well-defined three-dimensional architectures, which often include large cages or interconnected cavities. Materials such as PCN-222 and related frameworks have been studied for sensing applications [115] and for the thermocatalytic hydrogenation of CO_2 to methanol [116]. Their high surface areas, adjustable pore dimensions, and chemically tunable internal environments provide considerable flexibility for the development of efficient catalytic systems.

4.2.6. Institution Named MOFs

UiO-type metal–organic frameworks (MOFs) named based on University of Oslo were first reported by Cavka et al. and are based on $Zr_6(\mu_3\text{-}O)_4(\mu_3\text{-}OH)_4$ SBUs connected via dicarboxylate ligands into high connected and robust three-dimensional networks [117]. Among that family, UiO-66 is one of the most studied representatives. The presence of these interlinked cages and the exceptional thermal and chemical robustness of its framework, which is largely related to the strong coordination bonding between Zr (IV) and oxygen, makes the UiO-66 MOF unique [117]. Many other series of MOFs have also been synthesized and are widely known by acronyms that often derive from the names of the institutions where they were originally synthesized. Among them: HKUST-n, based on the HKUST-1 framework, from the Hong Kong University of Science and Technology [118], NOTT-n from the University of Nottingham [119], POST-n from Pohang University of Science and Technology [120], DUT-n from Dresden University of Technology [121], and CAU-n from Christian Albrechts University [122]. Another important category is bio-derived MOFs, generally known as Bio-MOFs, which have attracted interest for applications such as adsorption, catalysis, and environmental remediation [123]. These MOF families have been studied for CO_2 capture [124] and CO_2 conversion reaction because of their compositional diversity, tunable structures, and versatile pore environments [125].

The different MOF families provide distinct combinations of pore size, metal-node chemistry, linker functionality, and structural stability. Therefore, the choice of MOF family should be guided by the required balance between CO_2 adsorption, active-metal stabilization, mass transport, and resistance to reaction-induced degradation. Figure 5 shows structures of some MOF families, showing their different framework architectures and pore environments.

4.3. Preparation Strategies for MOF-Based Thermocatalysts

Thermocatalytic hydrogenation of CO_2 to methanol is commonly carried out at around 200–250 °C. Since many MOFs can retain structural stability at higher temperatures, in some cases up to approximately 400 °C, the selection of suitable MOF families and synthesis routes is important for preparing thermally robust MOF-based catalysts and nanoparticle composites.

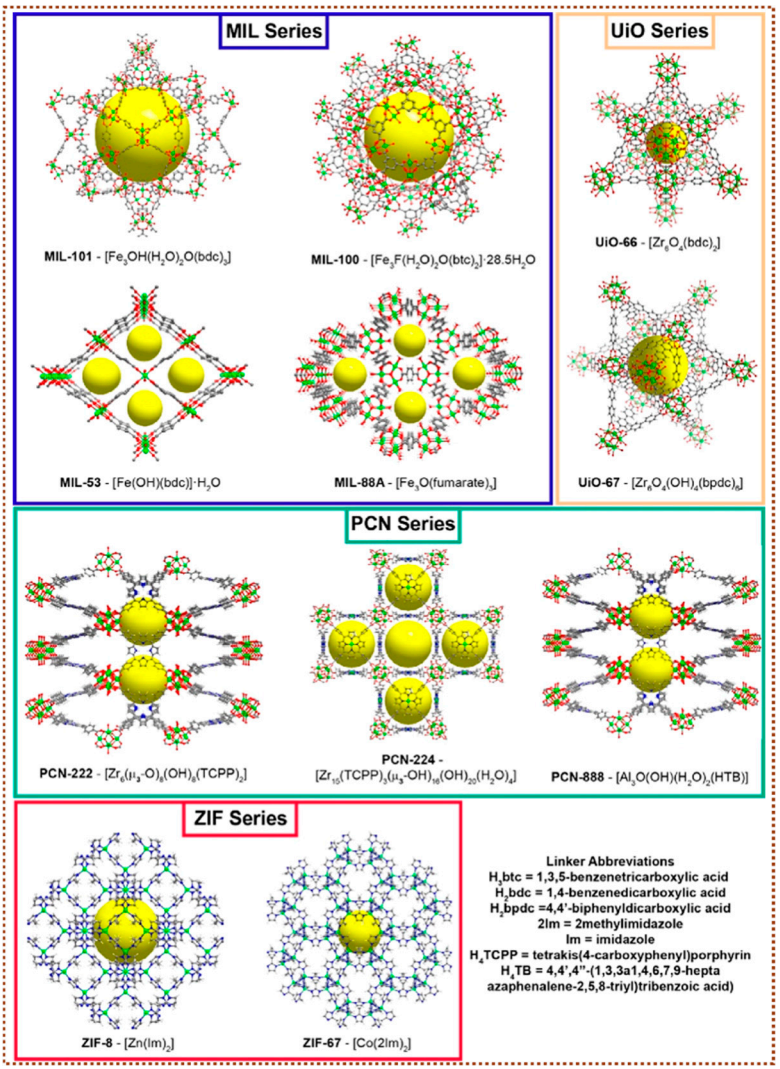

Figure 5. Representative structures of MIL-, UiO-, PCN- and ZIF-type MOFs, showing their different framework architectures and pore environments [126].

Several preparation strategies have been used to construct MOF-based thermocatalysts. These include coordination of nanoparticles with SBUs or organic linkers [127], encapsulation or impregnation of nanoparticles within MOF pores, grafting of nanoparticles onto MOF polymer matrices, and the use of MOFs as sacrificial templates. In the latter approach, the MOF is thermally treated to generate a derived catalytic material. Although this route may improve the dispersion of active components due to the ordered nature of the precursor, the final catalyst no longer fully retains the original MOF structure. Therefore, its suitability for industrial catalyst preparation still requires careful evaluation. The SBU plays a central role in determining the structural diversity, chemical functionality and permanent porosity of MOFs. Its chemical nature also enables post-synthetic linker or metal exchange, metallation and functionalization, thereby expanding the applications of MOFs in gas adsorption, separation and catalysis (Figure 6).

A range of synthesis routes has been explored to produce MOF-based catalysts for the hydrogenation of CO_2 to methanol. These include gas-phase infiltration, vapor deposition, nanoparticle encapsulation, hydrothermal synthesis, thermal decomposition, impregnation, and post-synthetic modification. An early example was reported by Müller and colleagues in 2008, who synthesized Cu/ZnO@MOF-5 through a gas-phase infiltration approach [108]. In this approach, small Cu nanoparticles of approximately 1–3 nm were first introduced

into MOF-5 to form Cu/MOF-5, followed by loading of nanocrystalline ZnO through hydrolysis/oxidation to obtain the final Cu/ZnO@MOF-5 catalyst. Although more stable MOFs are now available, MOF-5 was among the earliest widely studied frameworks and was also accessible on an industrial scale. Therefore, this work provided an important early demonstration of a relatively scalable route for MOF-based methanol synthesis catalysts.

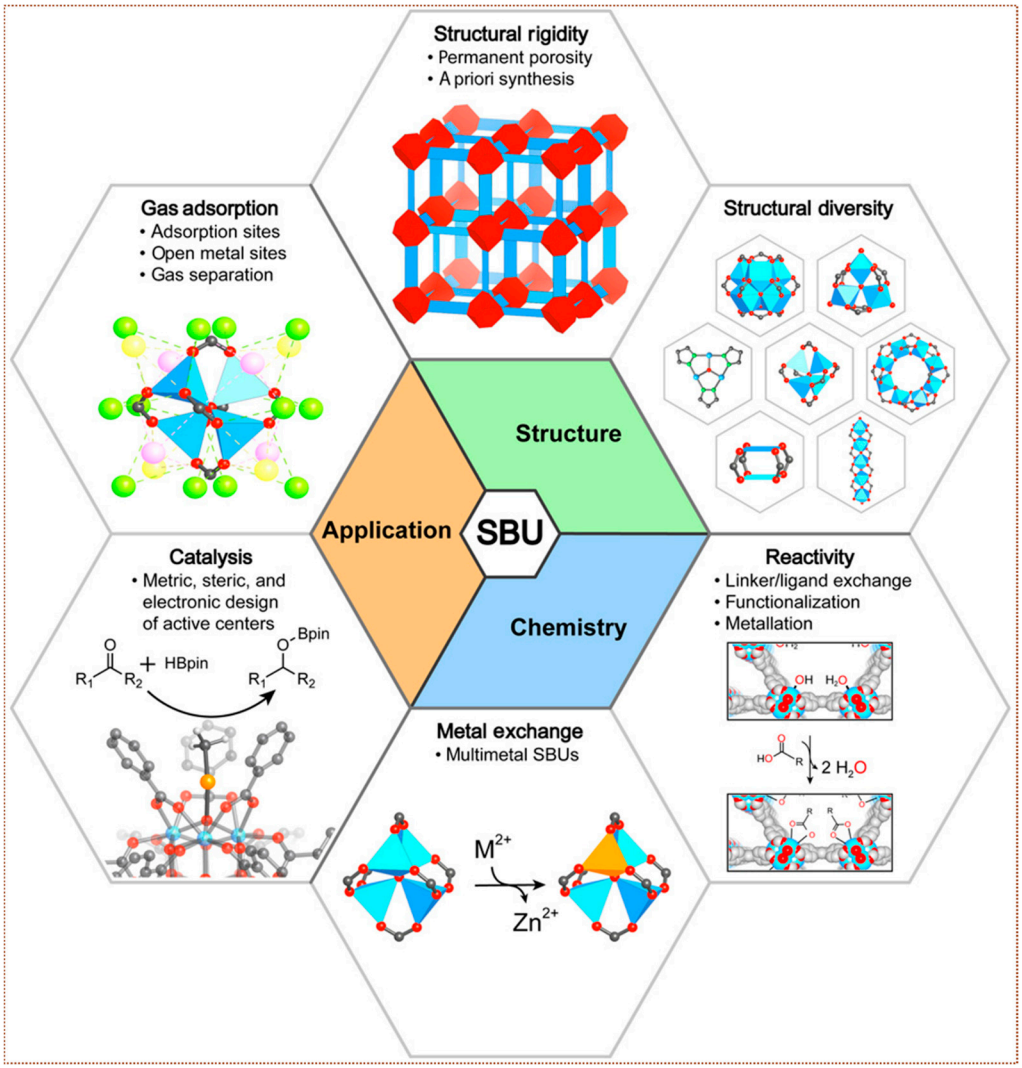

Figure 6. Role of secondary building units (SBUs) in determining the structure, chemistry and catalytic applications of MOFs [127].

To improve the thermal stability of MOF-supported catalysts, Nguyen et al. used metal–organic chemical vapor deposition to synthesize Cu@UiO-66 and Cu,ZnO@UiO-66 materials [128]. Subsequently, Rungtaweevoranit et al. developed a highly selective catalyst for methanol production by confining Cu nanocrystals within the UiO-66 framework [129]. The catalyst was prepared by dispersing pre-synthesized nanoparticles in a solution containing the MOF precursors, followed by heating at 65 °C for 15 h. The resulting mixture was then handled under a nitrogen atmosphere, freeze-dried, washed with DMF to remove residual and unreacted species, and finally dried under vacuum. This study represented one of the first examples of Cu nanocrystal encapsulation within UiO-66 for CO_2 hydrogenation to methanol.

Hydrothermal routes have also been used to prepare MOF-based hydrogenation catalysts. Zhao et al. synthesized Cu–Zn–Al-containing MOF/layered double hydroxide hybrid

materials while maintaining the desired metal ratio [130]. In this method, Cu–Al layered double hydroxide was first prepared hydrothermally, followed by in situ formation of Zn-BTC MOF from $Zn(NO_3)_2$ and BTC precursors in the LDH suspension. The resulting Cu–Al LDH/Zn-BTC catalyst combined Cu as the active hydrogenation metal with additional structural and promotional components.

Because Cu and ZrO_2 are well-known components in CO_2 hydrogenation catalysts, Zr-based MOFs have also been explored as precursors or supports for thermally stable systems. Zeng et al. converted UiO-66 into a hydrous zirconia-based material by treatment with CsOH and alkaline solutions, followed by incorporation of a nickel precursor [131]. The prepared $ZrO_x(OH)_y$-Cs-Ni catalyst achieved appreciable CO_2 conversion; however, the selectivity toward methanol was limited to about 4%. This result highlights that high CO_2 conversion alone is not sufficient; controlling product selectivity remains a major challenge.

MOFs have also been used as sacrificial templates to generate oxide-based catalysts with high dispersion and thermal stability. As an example, an In_2O_3/Co_3O_4 catalyst was obtained through the pyrolysis of cobalt-based ZIF-67 impregnated with an indium precursor. The resulting material delivered a methanol productivity of 0.65 gMeOH $gcat^{-1}$ h^{-1} at a methanol selectivity of 87% and remained stable during 100 h of continuous operation [132]. In another study, Cu@UiO-66 was employed as a sacrificial precursor for the preparation of porous Cu@ZrO_2 catalysts [133]. The porosity and defect-rich structure of UiO-66 promoted high Cu dispersion. In this synthesis, $CuAc_2{\cdot}H_2O$ was introduced into a defective UiO-66 suspension, followed by reduction with excess $NaBH_4$ and subsequent H_2 treatment at 500 °C to obtain a three-dimensional porous Cu-containing catalyst. These examples show that well-defined metal–metal oxide interfaces are important for achieving a stable and active catalyst for CO_2 hydrogenation.

Impregnation is another widely used method for preparing MOF-supported catalysts. For instance, Pt nanoparticles supported on UiO-67, prepared by impregnating UiO-67 with K_2PtCl_4 overnight, generating BPYDC–$PtCl_2$ active sites with a Pt loading of ~2.7 wt.% for CO_2 hydrogenation [111]. Kobayashi et al. prepared Cu/Zr-UiO-66-COOH and Cu/Zr-UiO-66-Hf catalysts with Cu loadings up to 19 wt.% [134]. In this strategy, part of the Zr^{4+} sites in UiO-66 were substituted with Ce^{4+}, which subsequently served as anchoring sites for Cu nanoparticles. More recently, Stawowy et al. reported Cu nanoparticles supported on mixed-metal Ce/Zr-UiO-66 for direct CO_2 hydrogenation, where Cu was introduced by incipient wetness impregnation [135]. To limit Cu aggregation and improve the spatial relationship between Cu and ZnO, Cu and ZnO nanostructures were coordinated within a UiO-bpy framework.

Post-synthetic functionalization is also an important strategy for designing MOF-based catalysts with targeted active sites. Strong interaction between the active metal and the MOF support has been identified as a key factor in improving catalytic performance. An et al. demonstrated this approach by anchoring Cu nanoparticles to the 2,2′-bipyridine-5,5′-dicarboxylate linker through post-synthetic metalation, followed by Zn coordination at the μ_3-OH sites of the SBUs [136]. This strategy produced a highly selective and stable MOF-based catalyst for CO_2 hydrogenation to methanol and represents one of the most effective approaches reported so far compared with benchmark catalysts.

In general, the preparation method strongly influences metal dispersion, nanoparticle size, metal-MOF interactions, and the final pore structure. No single synthesis route is universally optimal; the most suitable method depends on the required active-site architecture, framework stability, metal loading, and intended reaction conditions.

5. MOF-Based Thermocatalysts for CO_2 Hydrogenation to Methanol

5.1. Representative MOF-Based Catalyst Systems

The reported MOF-based catalysts for CO_2 hydrogenation to methanol conversion can generally be grouped into mono-, bi-, and trimetallic systems, oxide-containing composites, and MOF-derived catalysts supported on thermally stable frameworks and summarized in Table 5.

Table 5. Reported performance of MOF-based/MOF-derived catalysts for CO_2 hydrogenation reaction to methanol.

Catalyst	H_2/CO_2	T (°C)	P (bar)	GHSV (mL $gcat^{-1}$ h^{-1})	Time (h)	XCO_2 (%)	SCH_3OH (%)	STY (Reported Units)	Ref.
CuO-ZnO@ZIF-8	3	200	20	2400	na	14.6	93.4	409.78 mmol $kgcat^{-1}$ h^{-1}	[137]
20-Cu/ZrO_2	3	220	30	2400	na	5.1	45.9	0.63 mmol $gcat^{-1}$ h^{-1}	[138]
20-Cu@ZrO_2-U	3	220	30	12,000	na	7.0	78.7	7.38 mmol $gcat^{-1}$ h^{-1}	[138]
In_2O_3@ZrO_2	3	290	30	12,000	na	10.5	84.6	0.290 gMeOH $gcat^{-1}$ h^{-1}	[139]
Cr_2O_3/C-500-500	3	350	30	1200	na	16.8	98.1	1.18 mol $kgcat^{-1}$ h^{-1}	[140]
Cr_2O_3/C-500-600	3	350	30	1200	na	10.7	97.6	0.24 mol $kgcat^{-1}$ h^{-1}	[140]
CM-300	3	220	30	15,600	na	5.0	85.0	0.144 gMeOH $gcat^{-1}$ h^{-1}	[141]
CM-400	3	220	30	15,600	na	5.0	75.0	0.130 gMeOH $gcat^{-1}$ h^{-1}	[141]
Pd@In_2O_3-500	3	295	30	19,200	na	na	74.0	79.2 gMeOH $gcat^{-1}$ h^{-1}	[142]
Pd@In_2O_3-600	3	295	30	19,200	na	8.1	81.0	81.1 gMeOH $gcat^{-1}$ h^{-1}	[142]
In-Co-Zn/C-N	3	300	20	6000	na	7.0	77.7	3.30 mmol $gcat^{-1}$ h^{-1}	[143]
Cu-ZnO^{MOF}⊂ Al_2O_3	3	250	30	14,400	na	9.1	86.9	0.407 gMeOH $gcat^{-1}$ h^{-1}	[144]
Cu/ZnO_X@UiO-66	3	250	40	12,000	na	3.5	86.1	1.270 kg $kgCu^{-1}$ h^{-1}	[145]
ZnO/Zr_{12}-bpdc-Co	3	250	40	4500	na	16.0	>95.0	0.219 gMeOH $gcat^{-1}$ h^{-1}	[146]
ZnO/Zr_{12}-bpdc-Pd	3	250	40	4500	na	10.0	>50.0	0.098 gMeOH $gcat^{-1}$ h^{-1}	[146]
ZnO/Zr_{12}-bpdc	3	250	40	4500	na	7.5	>95.0	0.110 gMeOH $gcat^{-1}$ h^{-1}	[146]
3In@8Co(20)	4	300	50	15,600	na	19.0	62.0	0.480 gMeOH $gcat^{-1}$ h^{-1}	[132]
ZIF-67(Co)-In	na	300	50	na	20	na	80	0.65 gMeOH·$gcat^{-1}$ ·h^{-1}	[132]
3In@4Co(20)	na	300	50	na	3	20.5	na	0.5 gMeOH $gcat^{-1}$ h^{-1}	[132]
1In@6Co(20)	na	300	50	na	10	13.9	na	0.2 gMeOH $gcat^{-1}$ h^{-1}	[132]
1In@12Co(20)	na	300	50	na	40	11.1	na	0.05 gMeOH $gcat^{-1}$ h^{-1}	[132]
1In@23Co(20)	na	300	50	na	90	10.1	na	0.02 gMeOH $gcat^{-1}$ h^{-1}	[132]

Table 5. *Cont.*

Catalyst	H_2/CO_2	T (°C)	P (bar)	GHSV (mL $gcat^{-1}$ h^{-1})	Time (h)	XCO_2 (%)	SCH_3OH (%)	STY (Reported Units)	Ref.
UiO-66(Zr)	5	220	20	na	25	na	3.5	278 µmolMeOH/gCu/h	[135]
UiO-66(Ce/Zr)	5	220	20	na	25	na	28.7	275 µmolMeOH/gCu/h	[135]
Cu/UiO-66(Zr)	5	220	20	na	25	na	59	468 µmolMeOH/gCu/h	[135]
Cu/UiO-66(Ce/Zr)	5	220	20	na	25	na	56	468 µmolMeOH/gCu/h	[135]
CA-LDO	3	250	30	na	na	15	18	na	[130]
CZA-LDO	3	250	30	na	na	7	50	na	[130]
CA-ALDO	3	250	30	na	na	6	30	na	[130]
CZA-ALDO	3	250	30	na	na	7	50	na	[130]
$Cu^{II}(H_2PO_4)y$@RuUiO-66	3	150	na	na	24	1.1	99	na	[147]
UiO-67-Pt	na	170	na	na	4	na	3	na	[111]
UiO-67-Pt	na	170	na	na	4	na	19	na	[111]
PZ8-400	na	270	na	na	50	na	55	0.65 g $gcat^{-1}$ h^{-1}	[101]
PZ8-500	na	270	45	na	50	na	55	0.62 g $gcat^{-1}$ h^{-1}	[101]
CuZn@UiO-bpy	3	250	40	na	30	3.3	100	2.59 g_{MeOH} kg_{Cu}^{-1} h^{-1}	[19]
Cu@UiO-bpy	3	250	40	na	30	5.6	51.9	0.13 g_{MeOH} kg_{Cu}^{-1} h^{-1}	[19]
DSM-CuZn@UiO-bpy	3	250	40	na	30	7.1	94.6	0.58 g_{MeOH} kg_{Cu}^{-1} h^{-1}	[19]
DSM-CuZn@UiO-67	3	250	40	na	30	8.9	70.8	0.40 g_{MeOH} kg_{Cu}^{-1} h^{-1}	[19]
CuZn@MOF-253(Al)	3	250	40	na	30	8.7	93.2	0.27 g_{MeOH} kg_{Cu}^{-1} h^{-1}	[19]
Cu@UiO-66	na	175	10	na	na	na	na	na	[129]
Cu, ZnO@UiO-66	3	200	na	na	1	na	na	153.9 $\mu mol.g^{-1}.h^{-1}$	[128]
Cu@UiO-66	3	200	na	na	1	na	na	2.5 $\mu mol.g^{-1}.h^{-1}$	[128]
CuO/UiO-66, (≈4.3 wt% Cu)	3	240	30	18,000	na	2.2	80	2649 mg_{MeOH} gCu^{-1} h^{-1}	[148]
Cu/ZnO_x NPs/UiO-66	3	240	30	12,000	5	8.5	56.2	6.4 mmol g_cat^{-1} h^{-1}	[149]
Cu/UiO-66	3	250	32	na	50	0.7	na	4.68 molMeOH $molCu^{-1}$ h^{-1},	[22]
CuZn–BTC	3	250	40	1500	na	20.9	58.2	na	[113]
Cu@ZIF-8–ZnO/Cu	3	260	45	21,600	na	na	na	933 g kg_cat^{-1} h^{-1}	[102]
Pd/In_2O_3-MIL-68(In)	3	295	30	19,200	50	8.1	81	81.1 gMeOH h^{-1} gPd^{-1}	[142]
MIL-68(In)–In_2O_3	3	295	30	19,200	100	10.5	72.4	0.53 gMeOH h^{-1} $gcat^{-1}$	[150]
MIL-68(In)-derived In_2O_3	3	380	30	33,000	na	14.1	65	1.07 gMeOH h^{-1} $gcat^{-1}$	[151]

Table 5. *Cont.*

Catalyst	H_2/CO_2	T (°C)	P (bar)	GHSV (mL $gcat^{-1}$ h^{-1})	Time (h)	XCO_2 (%)	SCH_3OH (%)	STY (Reported Units)	Ref.
Pd–ZnO@ZIF-8	3	250	45	19,200	na	na	66–78	12.1–19.8 gMeOH gPd^{-1} h^{-1}	[104]
MIL-68@UiO-66-In_2O_3/ZrO_2	3	290	30	12,000	na	10.5	84.6	0.29 gMeOH $gcat^{-1}$ h^{-1}	[139]
Zr-BDC MOF-derived In_2O_3/ZrO_2	3	220	30	78,000	51	27.8	81.4	2.64 gMeOH $gcat^{-1}$ h^{-1}	[152]

na = not applicable.

To improve the catalytic efficiency of Cu-based MOFs for CO_2 hydrogenation to methanol, additional metals such as Zn have been introduced into the catalyst structure. In one study, Yang et al. synthesized a Cu/ZnO_x/UiO-66 catalyst through a dual-solvent approach [145]. At 250 °C and 4.0 MPa, this catalyst showed methanol space-time yields that were 5.5 and 8.5 times higher than those of commercial $Cu/ZnO/Al_2O_3$ and conventionally impregnated Cu/ZnO@UiO-66, respectively. The improved performance was attributed to the ability of the dual-solvent strategy to limit metal particle agglomeration and suppress phase separation between Cu and ZnO under high-temperature reaction conditions, thereby improving catalyst stability.

Mitsuka et al. synthesized Cu–ZnO/amUiO-66 composites by the spray drying method by integrating Cu-ZnO nanocomposites with amUiO-66 [153]. During CO_2 hydrogenation to methanol, Cu/amUiO-66 exhibited approximately three times higher activity than pristine UiO-66. Moreover, the Cu-ZnO/amUiO-66 composite increased methanol production by about 1.5 times compared with Cu/amUiO-66, confirming the promotional role of ZnO. More recently, Zhang et al. reported a flower-like CuO-ZnO@ZIF-8 catalyst with enhanced activity for methanol synthesis [137]. XPS and Raman analyses showed that this material contained a higher concentration of surface oxygen vacancies than the co-precipitated CuO-ZnO catalyst. These oxygen vacancies are considered important for CO_2 activation and subsequent hydrogenation to methanol.

MOFs can also be combined with conventional catalytic components such as Zn, Pt, and Cu to improve CO_2 hydrogenation performance. Gutterød et al. investigated UiO-67-Pt at 170 °C to clarify the influence of H_2O and the role of Zr nodes during CO_2 hydrogenation [111]. Using DFT calculations, steady-state and transient isotope exchange experiments, and H_2O co-feed studies, they showed that CH_4 and methanol formation rates increased with the defect density of Zr nodes. In another example, loading ZnO onto Zr-based MOFs enhanced selectivity of methanol up to 95%. Recently, Cu species anchored on Zr-oxo clusters inside a pore-confined MOF showed stable operation for more than 100 h in fixed-bed continuous-flow CO_2 hydrogenation, achieving an STY of 437.4 mL $gcat^{-1}$ h^{-1} at a high GHSV of 31,200 mL g^{-1} h^{-1} [116].

Besides serving directly as catalyst supports, MOFs can act as precursors for producing catalytic materials through pyrolysis. For example, mixtures of zeolitic-type MOFs, furfuryl alcohol, templating agents, and nanoporous carbon materials with high surface areas have been used to prepare porous carbon-based catalysts [154]. Similarly, $In_2O_3@Co_3O_4$ reticulated-shell nanocomposites were obtained through sequential pyrolysis and oxidative degradation of In-impregnated ZIF-67 [154]. An et al. synthesized UiO-bpy-Cu by introducing $CuCl_2$ into UiO-bpy in tetrahydrofuran, achieving a methanol selectivity of 62.7% [19]. The diffuse reflectance UV-vis-NIR spectrum of UiO-bpy-Cu showed metal-to-ligand charge-transfer and d–d transition bands at 470–530 nm and around 720 nm, respectively, confirming the coordination of Cu ions with bpydc linkers.

MOFs' tunable pore sizes, high surface areas, and functionalization possibilities make them useful as catalysts, catalyst supports, or precursors for MOF-derived materials [155]. However, despite these advantages, their use in practical applications is often restricted by limited stability under demanding reaction conditions. Under such environments, MOFs may undergo structural changes, lose surface area, or experience blockage of active sites [156]. To overcome these issues, it is important to adopt suitable synthesis and post-treatment methods that can maintain both the framework stability and porosity of MOFs during catalyst preparation and operation. For example, instead of conventional metal nitrate precursors, organometallic species have been used to introduce guest metals into MOF structures in order to minimize ligand oxidation during calcination and maintain framework stability [19]. Significant efforts have been devoted to improving the robustness of MOFs for catalytic applications [157]. Zhang et al. demonstrated that coating MOF-5 with a thin hydrophobic layer of polydimethylsiloxane significantly enhanced its resistance to moisture [158]. A similar strategy has been applied to HKUST-1, where the Cu(II) active sites retained their Lewis acidity even in humid environments during catalytic reactions such as cyanosilylation. Another effective approach involves the formation of protective coatings. Li et al. reported that applying a mesoporous silica ($mSiO_2$) layer around MOF structures improves both mechanical strength and chemical stability [159]. Building on this concept, a core–shell material, UiO-66@$mSiO_2$, was developed and subsequently used as a precursor for synthesizing yttria-stabilized zirconia with hierarchical porosity and enhanced resistance to chemical degradation [160]. These $mSiO_2$-coated materials have been used in a range of catalytic reactions as catalysts or supports. Moreover, Bao et al. reported a yolk–shell structure by embedding MOF nanoparticles in an $mSiO_2$ shell, which led to better protection of the catalyst core compared to traditional core–shell structures and prevented degradation during reactions such as CO_2 cycloaddition [157].

Koley et al. demonstrated how a MOF precursor can be used to engineer active oxide interfaces for CO_2 hydrogenation to methanol [152]. Pyrolysis of indium-impregnated Zr-BDC produced a ZrO_2-supported In_2O_3 catalyst with highly dispersed nanoparticles and interfacial oxygen vacancies. The authors propose that these vacancies promote CO_2 adsorption and activation, while nearby In and Zr sites help activate H_2 [152]. Similar studies on non-MOF oxide catalysts have also shown that oxygen vacancies and metal-oxide interfacial sites can strongly influence the formation of reactive species and catalytic activity. These studies showed that controlled oxygen-vacancy formation and surface oxygen species could be tuned through electronic-structure modification and confirmed using combined experimental and theoretical analyses [161–163]. In situ spectroscopy and DFT calculations support a formate-mediated pathway, in which adsorbed formate is progressively hydrogenated through carbon-containing intermediates to methanol. The study also highlights the need to optimize the In/Zr balance: excessive indium can stabilize formate too strongly and hinder its conversion. Under the reported conditions, the MOF-derived catalyst reached 81.4% methanol selectivity and a productivity of 2.64 gMeOH $gcat^{-1}$ h^{-1} in the gas phase; in liquid-phase hydrogenation, methanol selectivity reached 96.8% at 130 °C and 30 bar. These results illustrate how MOF-derived synthesis can control oxide dispersion, interfacial structure, and defect concentration to improve methanol-selective catalysis (Figure 7) [152].

Cu/ZrO_2 catalysts are very active for the hydrogenation of CO_2 to methanol at high temperature and pressure. This improved performance is linked to the strong interaction between Cu and the ZrO_2 support, a relatively low hydrophilicity and the suitable surface basicity of ZrO_2. This system has been widely studied in terms of the reaction mechanism, the role of zirconium dioxide crystal phases and the nature of the oxygen vacancies (Lewis acidic sites) [71,164]. In addition to oxide supports, zirconium-based MOFs (Zr-MOFs) have also been investigated as hosts for Cu-based catalysts for methanol synthesis [19,145].

Zr-MOFs offer a highly attractive platform for catalyst design due to the presence of a large number of coordination sites in their porous structure, arising from both the organic linkers and the metal-oxo clusters. This allows for homogeneous distribution of metals and the formation of very small metal nanoparticles, creating more accessible sites. Additionally, the pore confinement effect of MOFs restricts particle growth and improves the atom efficiency. However, drawbacks include that high-temperature treatments for preparing or operating the catalysts can cause partial MOF structure degradation, decrease in surface area, and aggregation of metal-oxo clusters [19,133]. A summary of process conditions and efficiency for methanol production of various MOF-based catalysts is shown in Table 5.

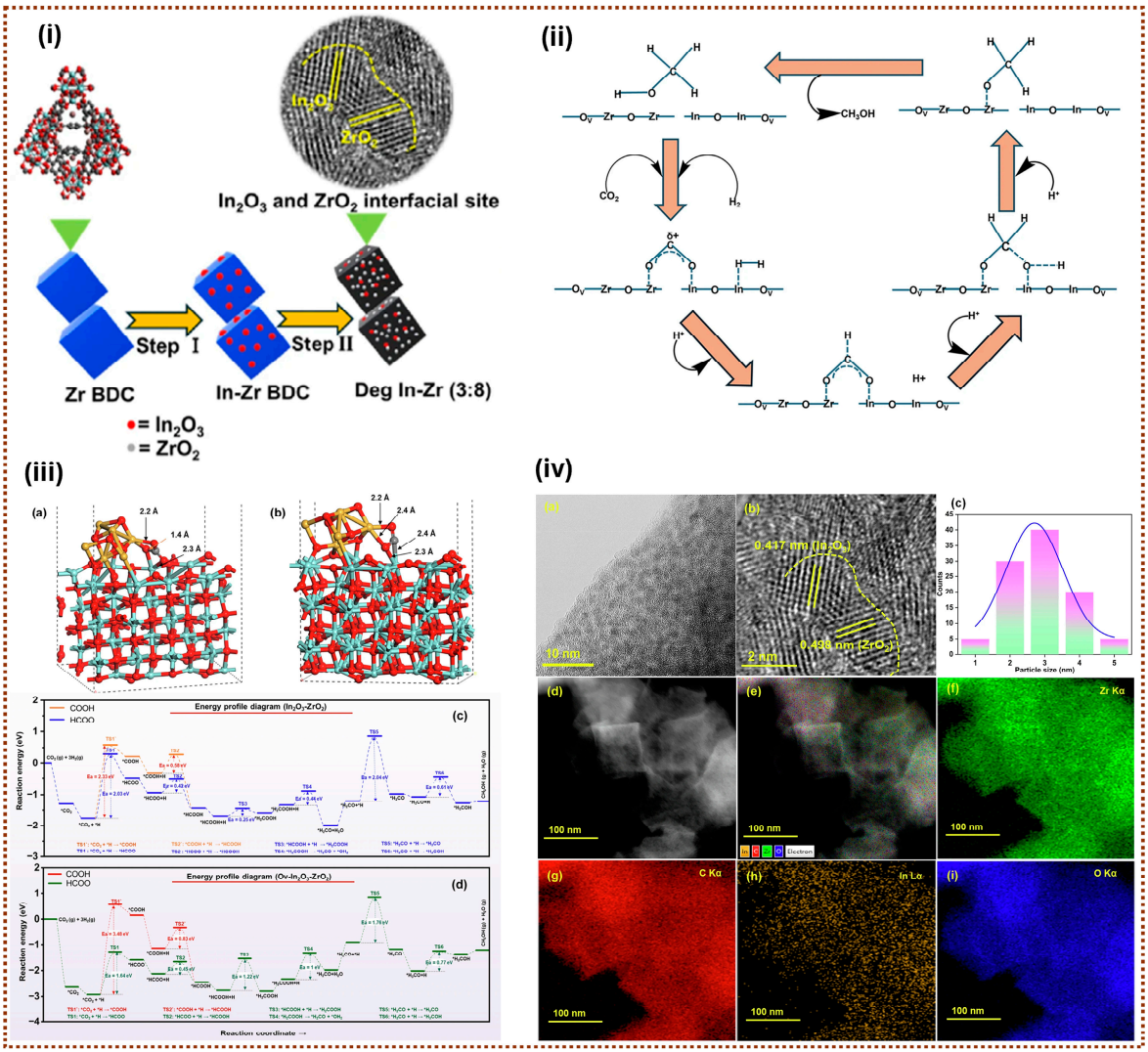

Figure 7. MOF-derived In_2O_3/ZrO_2 catalyst design and proposed CO_2 hydrogenation pathway. (**i**) Preparation of the Deg In–Zr (3:8) catalyst by indium impregnation of Zr-BDC followed by pyrolysis, forming In_2O_3/ZrO_2 interfacial sites. (**ii**) Proposed sequence of surface hydrogenation steps leading from activated CO_2 to methanol. (**iii**) DFT-optimized CO_2 adsorption structures and calculated energy profiles comparing the formate (*HCOO) and carboxylate (*COOH) pathways at the pristine interface and an oxygen-vacancy site. (**iv**) TEM/STEM images and elemental maps showing catalyst morphology and the distribution of C, In, O, and Zr [152].

In parallel with experimental investigations, computational methods have also been employed to examine MOF-based catalysts for the CO_2 hydrogenation to methanol. Using density functional theory calculations, Ye and Johnson designed a Lewis acid–base pair functionalized UiO-67 framework [147]. Their simulations indicated that H_2 undergoes

heterolytic dissociation within the MOF, generating a protonic hydrogen species at the Lewis basic site and a hydridic hydrogen species at the Lewis acidic site. These activated hydrogen species subsequently enable a sequence of elementary reactions leading toward methanol formation, as outlined below.

$$CO_2 \xrightarrow{+H_2} HCOOH \xrightarrow{+H_2} CH_2(OH)_2 \xrightarrow{+H_2O} CH_2O \xrightarrow{+H_2} CH_3OH$$

MOF-based supports, such as ZIF, UiO and MIL series, have unique structural and chemical features, which affect their catalytic performance. Although all these materials are highly porous and have high surface areas, they differ in pore sizes, pore connectivity, and chemical functionalities in the pores because of different metal nodes and organic linkers. These variations influence their catalytic performance, selectivity and stability. Overall, MOFs exhibit sufficient stability in various reaction environments and conditions. As indicated in Table 5, MOF-based catalysts for CO_2 hydrogenation to methanol generally perform in the temperature range of 200–380 °C and at pressures ranging from 1.8 to 4.5 MPa with competitive methanol production efficiencies. These results show that MOF-based catalysts can achieve competitive methanol production, but their performance cannot be compared only by CO_2 conversion or methanol selectivity. Metal loading, reaction temperature, pressure, space-time yield, feed composition, and catalyst stability must also be considered when evaluating different catalyst systems.

5.2. MNPs Encapsulated by MOFs for CO_2 Hydrogenation to Methanol

Metal–organic frameworks (MOFs) are a series of three-dimensional crystalline coordination polymers that have attracted significant interest since Yaghi's breakthrough in 1995 [165]. In 1999, the same group successfully synthesized $Zn_4O(BDC)_3{\cdot}(DMF)_8(C_6H_5Cl)$, MOF-5, where BDC = 1,4-benzenedicarboxylate, which is one of the most studied MOF systems [82].

MOFs are usually designed according to the principles of reticular chemistry, which involve three key elements: building units, desired network structures and isoreticular design [166]. The building units typically consist of SBUs, which are metal clusters or ions, and organic linkers [167]. The structural framework of MOFs is represented by topological nets that describe the arrangement of building units using node and link models [168]. These topologies provide a platform to design and build new MOF materials. Isoreticular chemistry, which involves modifying MOFs with different organic linkers or metal nodes while maintaining the same topology, is used to achieve this. This strategy facilitates fine-tuning of chemical and physical properties, enabling MOFs to be used for various applications under different conditions [169]. Overall, MOFs consist of metal-based SBUs connected by multidentate organic linkers, such as carboxylates, sulfonates, and phosphonates, to create ordered porous networks. This framework architecture provides defined spaces for nanoparticle encapsulation and enables control over the local catalytic environment.

To our knowledge, the early work by Yaghi et al. [129] represents one of the first attempts to utilize MOF-encapsulated metal nanoparticles (MNPs) for methanol synthesis via CO_2 hydrogenation. In their study, the catalytic behavior of Cu@UiO-66 was evaluated alongside conventional systems such as $Cu/ZnO/Al_2O_3$, Cu/ZrO_2 and Cu/UiO-66. Among these materials, Cu@UiO-66 demonstrated the highest methanol yield with complete selectivity toward CH_3OH. This superior performance was due to the close, strong interaction between Cu nanoparticles and the Zr-based SBUs, which generated a higher density of active sites for CO_2 conversion. The observed high selectivity toward methanol was linked to the intrinsic catalytic properties of the system, which suppressed CO formation. Furthermore, the study highlighted the role of Zr and Zn oxides as promoters, enhancing methanol productivity. These results are in agreement with the observations reported by Lercher

et al. and Castaño et al. [22,170], who identified Zn–O–Cu and Cu–O–Zr interfacial sites as key contributors to improved CO_2 activation and conversion efficiency. Whereas Yaghi et al. [129] used an intact UiO-66 structure, Lercher et al. [22] focused on incorporating Cu nanoparticles into a defective version of UiO-66. Under reaction conditions of 523 K and 32 bar, the catalyst exhibited approximately threefold higher activity compared to conventional $Cu/ZnO/Al_2O_3$ and Cu/ZrO_2 systems. This improvement was attributed to the presence of ultrasmall Cu nanoparticles and a higher concentration of Cu–O–Zr interfacial sites within the defective framework. Similarly, Castaño et al. [170] developed a Cu/ZIF-8 catalyst by ion-exchange incorporation of Cu at linker-defect sites. Under reaction conditions, the Cu species restructured into approximately 14 nm metallic nanoparticles stabilized within the Zn-based MOF. In situ DRIFTS supported a formate-mediated pathway, while DFT calculations indicated that CO_2 adsorption was more favorable at Cu-containing sites, including Cu–O–Zn interfacial sites, than at bare Zn or ZIF-8 sites. The authors associated this interfacial environment with suppression of the competing RWGS reaction and methanol selectivity exceeding 90%. At 523 K and 50 bar, the catalyst remained stable for over 150 h and achieved a space–time yield of 2.2 $gCH_3OH\ gmetal^{-1}\ h^{-1}$; the authors reported approximately twice the methanol productivity of a commercial Cu–Zn–Al catalyst (as shown in Figure 8). The findings reported by Yaghi et al. [129] were later reinforced by An et al. and co-workers [19], in which they show the successful incorporation of Cu/ZnO nanocatalysts into UiO-bpy frameworks resulted in a system with exceptional stability, exhibiting less than 10% loss in catalytic activity after 100 h of operation. Under reaction conditions of 250 °C and 4 MPa (H_2:CO_2 = 3:1), the catalyst achieved 100% methanol selectivity and a space time yield (STY) of 0.0809 mmol $MeOH{\cdot}gCu^{-1}h^{-1}$, surpassing the performance of both Cu@UiO-bpy and $Cu/ZnO/Al_2O_3$ reference catalysts. The enhanced catalytic performance can be attributed to the synergistic interaction among Cu, ZnO, and Zr_6 nodes, as well as the well-defined chemical environment provided by the MOF. A comparison between Cu/ZnOx@UiO-bpy and CuZn@MIL-253-Al further underscores the significance of pore size and confinement. UiO-bpy possesses narrow pore windows that limit nanoparticle growth, whereas MIL-253-Al features larger cavities that permit Cu nanoparticles to expand and migrate to the external surface, ultimately reducing methanol yield.

Encapsulation of nanoparticles within MOFs is commonly achieved through methods such as impregnation, co-precipitation, and deposition–precipitation, often referred to as the "ship-in-a-bottle" approach [171]. However, precise control over metal loading remains challenging, as precursor species may deposit on the external surface, leading to particle aggregation [172]. Li et al. [145] addressed this issue by introducing a double-solvent method for synthesizing Cu/ZnOx@UiO-66, which effectively prevented particle agglomeration and phase separation. The resulting catalyst exhibited excellent stability over 100 h of reaction, along with high methanol activity (STY = 1.27 $kg_{(MeOH)}kg(Cu)^{-1}\ h^{-1}$) 39.7) and selectivity (86.1%), significantly outperforming $Cu/ZnO/Al_2O_3$ under identical conditions [145]. In addition to Cu-based systems, Pd has also been extensively studied due to its strong ability to dissociate hydrogen. However, pure Pd tends to favor CO formation during CO_2 hydrogenation, resulting in low methanol selectivity. Alloying Pd with Zn has been shown to reverse this behavior, promoting methanol formation [173]. Tsang et al. [104] prepared a Pd–Zn alloy catalyst by anchoring Pd nanoparticles onto oxygen-deficient ZnO nanorods that were further coated with a ZIF-8 layer. They observed that increasing the thickness of the ZIF-8 layer enhanced CO_2 adsorption due to the formation of additional oxygen vacancies, although excessive thickness hindered PdZn alloy formation due to spatial confinement. An optimal balance was identified, resulting in maximum methanol productivity (space time yield = 19.8 g $g_{Pd}{}^{-1}\ h^{-1}$) at 563 K and 4.5 MPa after etching of

1 h. This study highlighted the importance of balancing alloy formation and surface defect concentration for optimal catalytic performance.

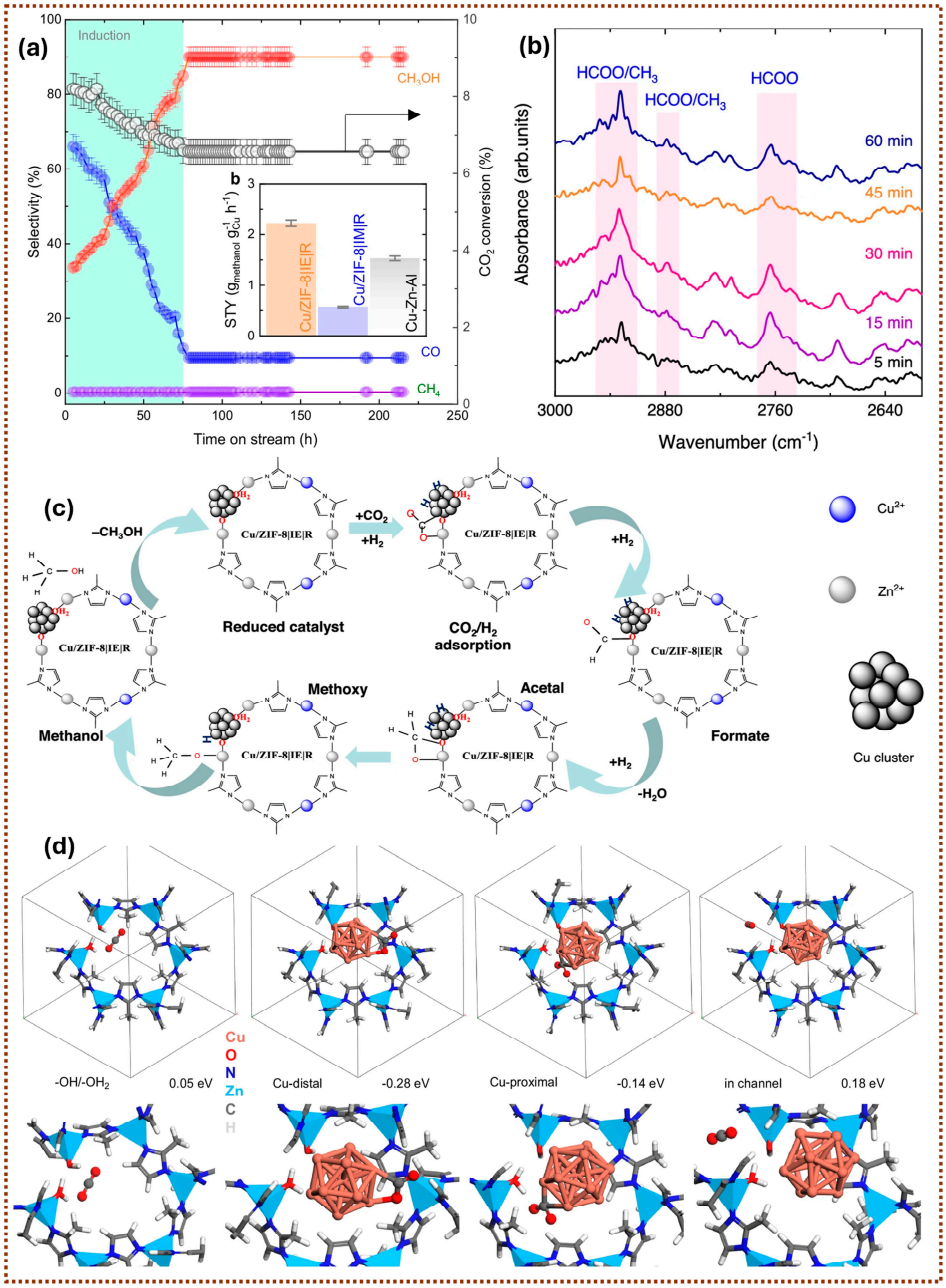

Figure 8. Catalytic performance and proposed CO_2 hydrogenation mechanism over Cu/ZIF-8. (**a**) Time-on-stream product selectivity and CO_2 conversion at 523 K and 50 bar with an 80% H_2/20% CO_2 feed; the inset compares the methanol space-time yield of ion-exchanged Cu/ZIF-8, impregnated Cu/ZIF-8, and commercial Cu–Zn–Al. (**b**) In situ DRIFT spectra recorded over 5–60 min at 523 K and 25 bar, showing bands assigned to formate and methoxy species. (**c**) Proposed formate-mediated pathway on reduced Cu/ZIF-8, proceeding through formate, acetal, and methoxy intermediates to methanol. (**d**) DFT-optimized CO_2 adsorption configurations and Gibbs free energies at the linker-defect, Cu-distal, Cu-proximal, and channel sites, respectively [170].

Methanol formation from CO_2 generally proceeds through two primary pathways: (i) the RWGS pathway, where CO_2 is first converted to CO and subsequently hydrogenated to methanol, and (ii) the formate pathway, in which HCOO* intermediates are formed and further reduced to methanol [45,174–176]. Catalysts such as Pd and Pt tend to promote

the RWGS reaction, leading to increased CO formation and reduced methanol selectivity [45,176,177]. Since CO accumulation can poison active sites and inhibit further reaction [178], achieving high methanol selectivity requires suppression of the RWGS pathway and stabilization of formate intermediates. To overcome this limitation, UiO-type MOFs rich in Zr-based Lewis acid sites have been explored for their capacity to stabilize HCOO* intermediates and facilitate their subsequent hydrogenation [179]. For example, Olsbye et al. [111] developed a Pt-encapsulated UiO-67 catalyst and evaluated its performance for CO_2 hydrogenation at 170 °C, 8 bar (H_2:CO_2 = 3:1). The defective UiO-67-Pt system exhibited higher methanol productivity (STY = 0.072 mmol MeOH·g$Cu^{-1}h^{-1}$) and selectivity (13%) compared to a less defective counterpart, attributed to the higher concentration of unsaturated Zr sites. These sites not only enhanced Pt–Zr interfacial interactions but also stabilized formate intermediates, facilitating methanol formation. Additionally, the presence of water was found to improve methanol selectivity by promoting desorption and suppressing formation of methane, as shown in Figure 9 [111].

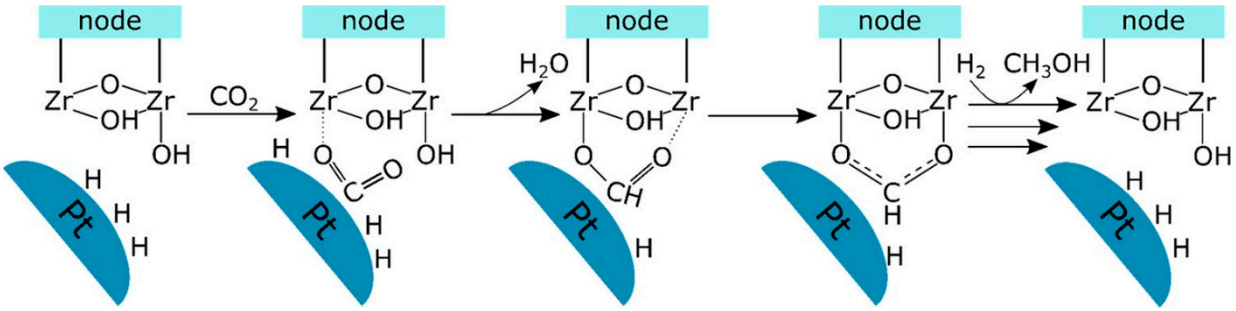

Figure 9. Schematic illustration for CO_2 hydrogenation mechanism highlighting the formation of the HCOO* intermediate at the Pt–Zr interfacial sites during methanol synthesis [111].

Overall, existing studies indicate that the most active sites in MNP@MOF systems are located at the interface between metal nanoparticles and MOF nodes, where synergistic effects enhance catalytic performance [180–182]. However, most theoretical investigations focus primarily on CO_2 activation, and a detailed understanding of how these synergistic effects influence each reaction step remains limited. As evident by comparisons in Table 6, several factors require further investigation, including the role of support structure, reaction conditions, and nanoparticle characteristics. For example, differences in catalytic performance between Cu/Zn@UiO-bpy and Cu/ZnO@UiO-66 demonstrate the significance of support effects. Similarly, variations between Cu@def-UiO-66 and Cu@UiO-66 underscore the impact of interfacial sites and defects. Furthermore, Pd–ZnO@ZIF-8 exhibits substantially higher methanol production than Cu@ZIF-8, which underscores the importance of metal selection and alloy formation in determining catalytic performance. Overall the confinement environment strongly influences CO_2 hydrogenation by controlling the immobilization and dispersion of active species within the porous structure. It also promotes heterogeneous recyclability, provides size-dependent active sites from the atomic to microscale, enhances interfacial electron transfer, and improves catalyst stability through encapsulation. These combined effects contribute to the improved catalytic performance of confined systems. These effects demonstrate that confinement is not merely a method for preventing nanoparticle sintering; it also regulates CO_2 adsorption, interfacial-site formation, intermediate stabilization, and mass transport. Thus, rational control of pore size, defect concentration, and metal–framework interactions is essential for improving the activity, methanol selectivity, and long-term stability of MOF-confined catalysts as illustrated in Figure 10.

Table 6. Performance of MOF-confined nanoparticle catalysts for hydrogenation of CO_2 to methanol.

Catalyst	Metal Loading (wt%)	Temp. (K)	Pressure (bar)	CO_2 Conversion (%)	Methanol Selectivity (%)	STY (g MeOH g_cat^{-1} h^{-1})	Ref.
Cu@UiO-66	1.0	448	10	10.2	100.0	0.042	[129]
Cu@def-UiO-66	1.4	523	32	<5.0	29.6	0.033	[22]
Pt@UiO-67	2.5	443	8	50.0	13.0	0.0192	[111,183]
Pd–ZnO@ZIF-8	3.0	563	45	3.5	78.0	0.594	[104]
Cu/ZnO@UiO-66	6.65	523	40	7.33	86.1	0.320	[145]
Cu/ZnO@UiO-bpy	6.9	523	40	10.2	98.0	0.018	[19]
Cu@ZIF-8	12.1	523	50	10.2	98.0	0.27	[170]

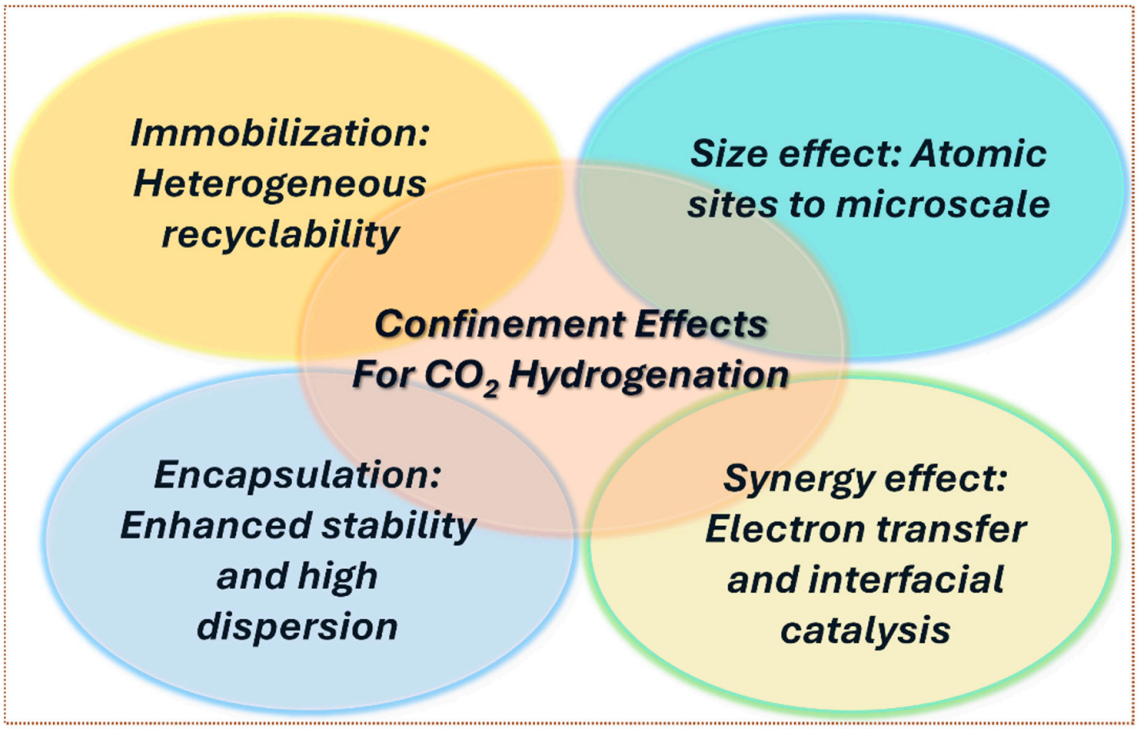

Figure 10. Summary of the confinement effects of MOFs and MOF-derived materials in CO_2 hydrogenation.

5.3. Comparison with Conventional Industrial Catalysts

Comparison with conventional supported catalysts can explain the performance of MOFs as catalyst supports for CO_2 hydrogenation to methanol. Recent reports on MOF-based and traditional catalysts tested under different reaction conditions are summarized in Table 7. The available data indicate that MOF-based systems may offer competitive and, in some cases, superior catalytic performance than in conventional counterparts. The enhancement is attributed primarily to their tunable pore structures, high surface areas, uniform dispersion of active species and formation of well-defined metal-support interfaces. Due to their excellent catalytic performance and highly tunable properties, MOFs are regarded as promising catalyst platforms for the future hydrogenation of CO_2 to methanol.

Table 7. Performance comparison of MOF-based and conventional supported catalysts for CO_2 hydrogenation to methanol.

Catalyst System	H_2/CO_2	Temp. (°C)	Pressure (bar)	Time (h)	CO_2 Conversion (%)	MeOH Selectivity (%)	TOF ($s^{-1} \times 10^{-3}$)	STY (gMeOH $kgcat^{-1}$ h^{-1})	Ref.
ML-MoS_2	3	260	60	NR	14.1	67.3	NR	1.880 gMeOH $gcat^{-1}$ h^{-1}	[184]
$Cu/ZnO/Al_2O_3$	3	260	60	NR	12.9	50.1	NR	1.240 gMeOH $gcat^{-1}$ h^{-1}	[184]
Cu@UiO-66	2	220	2	NR	NR	NR	NR	6.4	[133]
Cu/Al_2O_3	2	220	2	NR	NR	NR	NR	1.6	[133]
CuZn@UiObpy	3	250	40	100	3.3	100	NR	2.59	[19]
Cu@UiO-bpy	3	250	40	30	5.6	51.9	NR	0.13	[19]
DSMCuZn @UiObpy	3	250	40	30	7.1	94.6	NR	0.58	[19]
$Cu/ZnO/Al_2O_3$	3	250	40	100	NR	40	NR	1	[19]
$Cu/ZnO/Al_2O_3$	3	250	40	30	11.1	54.8	NR	0.83	[19]
Cu/UiO-66	NR	175	10	NR	NR	NR	04	NR	[129]
$Cu/ZnO/Al_2O_3$	NR	175	10	NR	NR	NR	01	NR	[129]
Cu/UiO-66	NR	200	10	NR	NR	NR	23	NR	[129]
$Cu/ZnO/Al_2O_3$	NR	200	10	NR	NR	NR	03	NR	[129]
Cu/UiO-66	NR	225	10	NR	NR	NR	10	NR	[129]
$Cu/ZnO/Al_2O_3$	NR	225	10	NR	NR	NR	03	NR	[129]
Cu/UiO-66	NR	250	10	NR	NR	NR	3	NR	[129]
$Cu/ZnO/Al_2O_3$	NR	250	10	NR	NR	NR	2.5	NR	[129]
(Cu/ZnO)@ MOF-5	NR	NR	1	NR	NR	NR	NR	6.8	[108]
$Cu/ZnO/Al_2O_3$	NR	NR	NR	NR	NR	NR	NR	12	[108]

Industrial methanol synthesis catalysts like $Cu/ZnO/Al_2O_3$ are mature, cost-effective and highly optimized but were originally developed for syngas-rich feeds and can be limited under CO_2-rich conditions by water formation, sintering and loss of active Cu-ZnO interfacial sites. MOF-based catalysts have many advantages, including the encapsulation of ultrasmall metal particles, the formation of well-defined metal-node interfaces, tunable hydrophobicity for controlling water, and defect sites for CO_2 adsorption and stabilization of intermediates. These features can improve methanol selectivity and stability in some systems but have not yet exceeded industrial catalysts in terms of productivity, lifetime, mechanical robustness or cost [185,186].

Thus, MOF-based catalysts should not be regarded as mere substitutes for classical oxides but as design platforms to find active-site architectures hard to obtain in classical supports. The most promising directions include MOF-confined Cu/ZnO_x interfaces, PdZn and Pt-Zr interfacial sites, defect-rich Zr-MOFs, MOF-derived mixed oxides, and hybrid materials that combine MOF confinement with oxide stability. Meaningful comparison with industrial catalysts requires standardized reporting of CO_2 conversion, methanol selectivity, STY, metal loading, catalyst mass, feed composition, pressure, temperature, and time-on-stream.

6. Challenges, Future Directions and Conclusions

Although CO_2 hydrogenation to methanol has advanced considerably, MOF-based catalysts still face several barriers before practical application. The most important target is operation under milder conditions, especially lower temperature (<200 °C) to improve methanol yield and lower pressure to reduce compression costs for renewable H_2. Liquid-phase methanol synthesis and intensified reactor designs may also help improve heat management and decentralized production [187,188]. Achieving these goals requires catalysts that combine strong CO_2/H_2 activation with suppression of RWGS and methanation.

Among the reported studies, the study of the Gascon group [132] represents one of the most remarkable works that have shown the rates of methanol production of about 650 g/kg h^{-1} with a selectivity of about 87% and a stable work of more than 100 h. This stability is encouraging, but it is not as long as the industrial demands. Moreover, its productivity is similar to that of the CZA catalysts, but not yet the dramatic performance improvement required to enable next-generation low-temperature processes. Notably, the main application of MOFs in this method was to create a well-dispersed catalytic species during pyrolysis, as opposed to using the inherent structural characteristics of the MOFs. This restricts the benefits that are normally attributed to MOFs. Other issues are associated with the use of indium-based active phases that pose difficulties in terms of cost, safety, and scaled operation and the difficulty in MOF-derived catalyst synthesis. The other approach is to insert Cu or Cu/ZnO nanoparticles into MOF structures to sinter. Although confinement effects and enhanced stability of particles are advantages of this method, much of the specific character of MOFs has not been harnessed. As an illustration, there are yet to be fully explored opportunities to tune the chemical environment by functionalizing the linkers, to design cooperative metal sites to carry out synergistic catalysis, to control hydrophobicity to inhibit water, and to improve CO adsorption around the active sites. These weaknesses demonstrate that there is room to enhance the performance of catalysts by better designing MOFs. Application-wise, there are also a number of practical issues, which should be tackled. The thermal stability of organic linkers is another drawback of MOFs that is often mentioned to be limited due to the fact that organic linkers may be destroyed at high temperatures. Nonetheless, the low-temperature methanol production (below 200 °C) is the desired goal, and, therefore, the degradation at the required temperature might not be the major issue; instead, the stability under the reaction conditions should be taken into account. Also, interest in employing methanol synthesis in conjunction with the subsequent conversion processes, like olefins or aromatics production through zeolitic catalysts, is growing [189–193]. MOFs in this case may provide a distinct possibility to integrate several catalytic functions in a single material. Nevertheless, their practical use can be restricted by problems like the deactivation of catalysts (because of the deposition of heavy products) and the necessity of their regeneration.

Future MOF catalyst design should move beyond using MOFs only as sacrificial templates. More emphasis is needed on using intrinsic MOF features such as linker functionalization, defect engineering, pore hydrophobicity, and spatially isolated metal nodes. These features can be used to tune CO_2 adsorption, stabilize HCOO* or COOH* intermediates, control water desorption, and create cooperative metal-node active sites. In particular, the influence of confinement and interfacial engineering on methanol selectivity is demonstrated in Cu/ZnOx @MOF, Cu/Zr-MOF, PdZn@ZIF, Pt@UiO and MOF-derived In_2O_3-based systems.

There are some improvement strategies that are especially important. First, the defect density should be optimized rather than maximized, because the missing linkers may improve CO_2 adsorption and interfacial contact but also weaken the framework stability. Second, hydrophobic linkers or coatings should be explored to reduce water-induced deactivation. Third, single-atom and dual-site catalysts anchored at MOF nodes may provide precise control of H_2 activation and CO_2 hydrogenation steps. Fourth, MOF-derived mixed oxides should be designed so that the beneficial dispersion created by the MOF precursor is retained after pyrolysis. Finally, catalyst development should be supported by operando spectroscopy and theoretical modeling to identify the actual active sites under reaction conditions.

High-pressure operation is another challenge because CO_2 hydrogenation to methanol is favored by pressure, whereas some MOFs may undergo structural distortion, pore collapse,

or loss of surface area under combined pressure, heat, and water exposure. Metal loading may also modify the MOF structure and decrease the accessible porosity [19,111], so the catalyst preparation is a trade-off between the metal content and the framework integrity. The scalable synthesis continues to be a serious practical issue, with the electrochemical, microwave-assisted, mechanochemical, spray-drying, and flow-based routes considered promising for enhancing the reproducibility and lowering the cost [194].

Besides methanol, MOF-based catalysts could also be interesting for stepwise CO_2 conversion to higher-value products like light olefins and higher alcohols. However, further work should be aimed at long-term stability, standard performance parameters, regeneration behavior, water resistance, and direct comparison with industrial benchmark catalysts for the present methanol-centered application under the same set of conditions. Such guidelines will indicate whether MOF-based systems can be further developed from promising lab materials to practical CO_2-to-methanol catalysts.

In this review, we summarize the state-of-the-art and recent advances of MOF-based and MOF-derived catalysts in thermocatalytic CO_2 conversion, with particular attention on CO_2 hydrogenation to methanol. The reviewed literature demonstrates that the adjustable metal nodes, organic linkers, pore structures, defects, and confinement environment of MOFs offer unique opportunities to modulate catalytic activity and product selectivity. These properties may increase CO_2 adsorption and metal dispersion, stabilize small nanoparticles or single metal sites, and develop active metal–support interfaces that promote methanol synthesis. Despite these advantages, framework stability, mass transport, water resistance, and nanoparticle sintering remain important limitations for practical application. Therefore, emphasis in future work should be on water-stable frameworks, stronger metal–linker bonds, hierarchical porosity, larger pore channels, protective core–shell structures, and integration with mechanically stable supports.

Conventional MOF synthesis methods often require expensive precursors, toxic solvents, long reaction times, and several purification steps. Consider some alternative, greener routes along these lines, such as aqueous synthesis, microwave-assisted synthesis, mechanochemistry and continuous-flow production that might result in reduced solvent consumption, reduced energy usage, reduced manufacturing cost, and increased reproducibility. Using porous metals, metal foams, oxides and structured supports could still be further improved to ensure better catalyst handling, heat transfer and mechanical strength, and continuous operation. Future research should prioritize MOF catalysts that operate at temperatures below 250 °C and pressures below 3 MPa while maintaining high methanol selectivity, productivity, and long-term stability. Promising directions include defect-controlled Zr-based MOFs, alternative stable metal nodes, hydrophobic linkers, single-atom and dual-site catalysts, confined Cu/ZnO_x and PdZn interfaces, and MOF-derived mixed oxides with preserved nanoscale dispersion. Operando characterization, computational modeling, standardized performance reporting, techno-economic assessment, and long-duration testing are also required to identify the true active phases and allow meaningful comparison between catalysts.

Overall, MOFs provide a versatile platform for CO_2 to methanol conversion, but their future success will rely on the integration of molecular catalyst design based on scalable synthesis and efficient reactor engineering. To be translated into energy-efficient and economically feasible CO_2 valorization technologies, positively evolving laboratory results need to be propagated by suitably dealing with issues of stability, mass transport, reagent preparation cost, and process integration.

Funding: This research received no external funding.

Data Availability Statement: No new data were created or analyzed in this study. Data sharing is not applicable to this article.

Acknowledgments: The author gratefully acknowledges the Department of Chemistry, King Fahd University of Petroleum and Minerals (KFUPM), Dhahran, Saudi Arabia, for providing the research facilities and institutional support that made this work possible. During the preparation of this manuscript, the author used ChatGPT 5.6 for the purposes of generating the catalyst–support image in Figure 2. The authors have reviewed and edited the output and take full responsibility for the content of this publication.

Conflicts of Interest: The author declares no conflict of interest.

References

1. Sanz-Pérez, E.S.; Murdock, C.R.; Didas, S.A.; Jones, C.W. Direct capture of CO_2 from ambient air. *Chem. Rev.* **2016**, *116*, 11840–11876. [CrossRef] [PubMed]
2. Dabirifar, Z.; Khadempir, S.; Kardan, A.; Karaman, C.; Karaman, O.; Yola, M.L. Design of Co-Sn bimetallic nanoalloys as electrocatalyst for alkaline methanol oxidation reaction: Exploring the effect of electroactivation process. *Fuel* **2022**, *319*, 123727. [CrossRef]
3. Yao, B.; Xiao, T.; Makgae, O.A.; Jie, X.; Gonzalez-Cortes, S.; Guan, S.; Kirkland, A.I.; Dilworth, J.R.; Al-Megren, H.A.; Alshihri, S.M. Transforming carbon dioxide into jet fuel using an organic combustion-synthesized Fe-Mn-K catalyst. *Nat. Commun.* **2020**, *11*, 6395. [CrossRef] [PubMed]
4. Andrew, R.M. Global CO_2 emissions from cement production. *Earth Syst. Sci. Data* **2018**, *10*, 195–217. [CrossRef]
5. Lu, Q.; Rosen, J.; Zhou, Y.; Hutchings, G.S.; Kimmel, Y.C.; Chen, J.G.; Jiao, F. A selective and efficient electrocatalyst for carbon dioxide reduction. *Nat. Commun.* **2014**, *5*, 3242. [CrossRef] [PubMed]
6. Srinivas, G.; Krungleviciute, V.; Guo, Z.-X.; Yildirim, T. Exceptional CO_2 capture in a hierarchically porous carbon with simultaneous high surface area and pore volume. *Energy Environ. Sci.* **2014**, *7*, 335–342. [CrossRef]
7. Didas, S.A.; Choi, S.; Chaikittisilp, W.; Jones, C.W. Amine–oxide hybrid materials for CO_2 capture from ambient air. *Acc. Chem. Res.* **2015**, *48*, 2680–2687. [CrossRef] [PubMed]
8. Rafiee, A.; Khalilpour, K.R.; Milani, D.; Panahi, M. Trends in CO_2 conversion and utilization: A review from process systems perspective. *J. Environ. Chem. Eng.* **2018**, *6*, 5771–5794. [CrossRef]
9. Porosoff, M.D.; Yan, B.; Chen, J.G. Catalytic reduction of CO_2 by H_2 for synthesis of CO, methanol and hydrocarbons: Challenges and opportunities. *Energy Environ. Sci.* **2016**, *9*, 62–73. [CrossRef]
10. Perathoner, S.; Centi, G. Catalysis for solar-driven chemistry: The role of electrocatalysis. *Catal. Today* **2019**, *330*, 157–170. [CrossRef]
11. Wang, J.-J.; Li, X.-P.; Cui, B.-F.; Zhang, Z.; Hu, X.-F.; Ding, J.; Deng, Y.-D.; Han, X.-P.; Hu, W.-B. A review of non-noble metal-based electrocatalysts for CO_2 electroreduction. *Rare Met.* **2021**, *40*, 3019–3037. [CrossRef]
12. Zhang, W.; Jin, Z.; Chen, Z. Rational-designed principles for electrochemical and photoelectrochemical upgrading of CO_2 to value-added chemicals. *Adv. Sci.* **2022**, *9*, 2105204. [CrossRef] [PubMed]
13. Sha, F.; Han, Z.; Tang, S.; Wang, J.; Li, C. Hydrogenation of Carbon Dioxide to Methanol over Non− Cu-based Heterogeneous Catalysts. *ChemSusChem* **2020**, *13*, 6160–6181. [CrossRef] [PubMed]
14. Sakata, Y.; Tamaura, Y.; Imamura, H.; Watanabe, M. Preparation of a new type of CaSiO3 with high surface area and property as a catalyst support. In *Studies in Surface Science and Catalysis*; Elsevier: Amsterdam, The Netherlands, 2006; Volume 162, pp. 331–338.
15. Kumar, P.; Vellingiri, K.; Kim, K.-H.; Brown, R.J.; Manos, M.J. Modern progress in metal-organic frameworks and their composites for diverse applications. *Microporous Mesoporous Mater.* **2017**, *253*, 251–265. [CrossRef]
16. Guntern, Y.T.; Vavra, J.; Karve, V.V.; Varandili, S.B.; Segura Lecina, O.; Gadiyar, C.; Buonsanti, R. Synthetic tunability of colloidal covalent organic framework/nanocrystal hybrids. *Chem. Mater.* **2021**, *33*, 2646–2654. [CrossRef]
17. Ranocchiari, M.; van Bokhoven, J.A. Catalysis by metal–organic frameworks: Fundamentals and opportunities. *Phys. Chem. Chem. Phys.* **2011**, *13*, 6388–6396. [CrossRef] [PubMed]
18. Chavan, S.; Vitillo, J.G.; Gianolio, D.; Zavorotynska, O.; Civalleri, B.; Jakobsen, S.; Nilsen, M.H.; Valenzano, L.; Lamberti, C.; Lillerud, K.P. H_2 storage in isostructural UiO-67 and UiO-66 MOFs. *Phys. Chem. Chem. Phys.* **2012**, *14*, 1614–1626. [CrossRef] [PubMed]
19. An, B.; Zhang, J.; Cheng, K.; Ji, P.; Wang, C.; Lin, W. Confinement of ultrasmall cu/zno x nanoparticles in metal–organic frameworks for selective methanol synthesis from catalytic hydrogenation of CO_2. *J. Am. Chem. Soc.* **2017**, *139*, 3834–3840. [CrossRef] [PubMed]

20. Zhao, Z.-W.; Zhou, X.; Liu, Y.-N.; Shen, C.-C.; Yuan, C.-Z.; Jiang, Y.-F.; Zhao, S.-J.; Ma, L.-B.; Cheang, T.-Y.; Xu, A.-W. Ultrasmall Ni nanoparticles embedded in Zr-based MOFs provide high selectivity for CO_2 hydrogenation to methane at low temperatures. *Catal. Sci. Technol.* **2018**, *8*, 3160–3165. [CrossRef]
21. Abdel-Mageed, A.M.; Rungtaweevoranit, B.; Parlinska-Wojtan, M.; Pei, X.; Yaghi, O.M.; Behm, R.J.r. Highly active and stable single-atom Cu catalysts supported by a metal–organic framework. *J. Am. Chem. Soc.* **2019**, *141*, 5201–5210. [CrossRef] [PubMed]
22. Zhu, Y.; Zheng, J.; Ye, J.; Cui, Y.; Koh, K.; Kovarik, L.; Camaioni, D.M.; Fulton, J.L.; Truhlar, D.G.; Neurock, M. Copper-zirconia interfaces in UiO-66 enable selective catalytic hydrogenation of CO_2 to methanol. *Nat. Commun.* **2020**, *11*, 5849. [CrossRef] [PubMed]
23. Yu, J.; Liu, S.; Mu, X.; Yang, G.; Luo, X.; Lester, E.; Wu, T. Cu-ZrO_2 catalysts with highly dispersed Cu nanoclusters derived from ZrO2@ HKUST-1 composites for the enhanced CO_2 hydrogenation to methanol. *Chem. Eng. J.* **2021**, *419*, 129656. [CrossRef]
24. Furukawa, H.; Ko, N.; Go, Y.B.; Aratani, N.; Choi, S.B.; Choi, E.; Yazaydin, A.Ö.; Snurr, R.Q.; O'Keeffe, M.; Kim, J. Ultrahigh porosity in metal-organic frameworks. *Science* **2010**, *329*, 424–428. [CrossRef] [PubMed]
25. Wang, H. Nanostructure@ metal-organic frameworks (MOFs) for catalytic carbon dioxide (CO_2) conversion in photocatalysis, electrocatalysis, and thermal catalysis. *Nano Res.* **2022**, *15*, 2834–2854. [CrossRef]
26. Pan, X.; Xu, J.; Wang, Y.; Ma, M.; Liao, H.; Sun, H.; Fan, M.; Wang, K.; Sun, K.; Jiang, J. A new perspective on hydrogenation of CO_2 into methanol over heterogeneous catalysts. *Prog. Nat. Sci. Mater. Int.* **2024**, *34*, 482–494. [CrossRef]
27. Wen, H.; Liao, H.; Pan, X.; Sun, K.; Jiang, J.; Liao, Y.; Yuan, X.; Sun, H. Recent advances in carbon-based catalysts for CO_2 hydrogenation toward circular economy. *Carbon Capture Sci. Technol.* **2025**, *16*, 100482. [CrossRef]
28. Liao, Y.; Li, S.; Xie, Y.; Wen, H.; Weng, B.; Sun, H.; Yuan, X. Carbon material-driven photothermal CO_2 reduction for catalyzing a circular carbon economy. *J. Mater. Chem. A* **2026**, *14*, 12566–12588. [CrossRef]
29. Wang, J.; Jia, C.-S.; Li, C.-J.; Peng, X.-L.; Zhang, L.-H.; Liu, J.-Y. Thermodynamic Properties for Carbon Dioxide. *ACS Omega* **2019**, *4*, 19193–19198. [CrossRef] [PubMed]
30. Li, X.; Ke, J.; Li, R.; Li, P.; Ma, Q.; Zhao, T.-S. Research progress of hydrogenation of carbon dioxide to ethanol. *Chem. Eng. Sci.* **2023**, *282*, 119226. [CrossRef]
31. Etim, U.J.; Zhang, C.; Zhong, Z. Impacts of the catalyst structures on CO_2 activation on catalyst surfaces. *Nanomaterials* **2021**, *11*, 3265. [CrossRef] [PubMed]
32. Niu, J.; Ran, J.; Ou, Z.; Du, X.; Wang, R.; Qi, W.; Zhang, P. CO_2 dissociation over PtxNi4− x bimetallic clusters with and without hydrogen sources: A density functional theory study. *J. CO_2 Util.* **2016**, *16*, 431–441. [CrossRef]
33. Sakakura, T.; Choi, J.-C.; Yasuda, H. Transformation of carbon dioxide. *Chem. Rev.* **2007**, *107*, 2365–2387. [CrossRef] [PubMed]
34. Ma, J.; Sun, N.; Zhang, X.; Zhao, N.; Xiao, F.; Wei, W.; Sun, Y. A short review of catalysis for CO_2 conversion. *Catal. Today* **2009**, *148*, 221–231. [CrossRef]
35. Olah, G.A. Beyond Oil and Gas: The Methanol Economy. *Angew. Chem. Int. Ed.* **2005**, *44*, 2636–2639. [CrossRef] [PubMed]
36. Shih, A.J.; Monteiro, M.C.O.; Dattila, F.; Pavesi, D.; Philips, M.; da Silva, A.H.M.; Vos, R.E.; Ojha, K.; Park, S.; van der Heijden, O.; et al. Water electrolysis. *Nat. Rev. Methods Primers* **2022**, *2*, 84. [CrossRef]
37. Jia, C.; Gao, J.; Dai, Y.; Zhang, J.; Yang, Y. The thermodynamics analysis and experimental validation for complicated systems in CO_2 hydrogenation process. *J. Energy Chem.* **2016**, *25*, 1027–1037. [CrossRef]
38. He, Y.; Liu, S.; Fu, W.; Wang, C.; Mebrahtu, C.; Sun, R.; Zeng, F. Thermodynamic Analysis of CO_2 Hydrogenation to Higher Alcohols (C2–4OH): Effects of Isomers and Methane. *ACS Omega* **2022**, *7*, 16502–16514. [CrossRef] [PubMed]
39. Tkachenko, O.P.; Klementiev, K.V.; Löffler, E.; Ritzkopf, I.; Schüth, F.; Bandyopadhyay, M.; Grabowski, S.; Gies, H.; Hagen, V.; Muhler, M.; et al. The structure of zinc and copper oxide species hosted in porous siliceous matrices. *Phys. Chem. Chem. Phys.* **2003**, *5*, 4325–4334. [CrossRef]
40. Tsoukalou, A.; Abdala, P.M.; Armutlulu, A.; Willinger, E.; Fedorov, A.; Müller, C.R. Operando X-ray Absorption Spectroscopy Identifies a Monoclinic ZrO2:In Solid Solution as the Active Phase for the Hydrogenation of CO_2 to Methanol. *ACS Catal.* **2020**, *10*, 10060–10067. [CrossRef]
41. Yang, M.; Yu, J.; Zimina, A.; Sarma, B.B.; Pandit, L.; Grunwaldt, J.-D.; Zhang, L.; Xu, H.; Sun, J. Probing the Nature of Zinc in Copper-Zinc-Zirconium Catalysts by Operando Spectroscopies for CO_2 Hydrogenation to Methanol. *Angew. Chem.* **2023**, *135*, e202216803. [CrossRef]
42. Bale, C.W.; Bélisle, E.; Chartrand, P.; Decterov, S.A.; Eriksson, G.; Gheribi, A.E.; Hack, K.; Jung, I.H.; Kang, Y.B.; Melançon, J.; et al. Reprint of: FactSage thermochemical software and databases, 2010–2016. *Calphad* **2016**, *55*, 1–19. [CrossRef]
43. Sehested, J. Industrial and scientific directions of methanol catalyst development. *J. Catal.* **2019**, *371*, 368–375. [CrossRef]
44. Salami, R.; Zeng, Y.; Han, X.; Rohani, S.; Zheng, Y. Exploring catalyst developments in heterogeneous CO_2 hydrogenation to methanol and ethanol: A journey through reaction pathways. *J. Energy Chem.* **2025**, *101*, 345–384. [CrossRef]
45. Kattel, S.; Liu, P.; Chen, J.G. Tuning selectivity of CO_2 hydrogenation reactions at the metal/oxide interface. *J. Am. Chem. Soc.* **2017**, *139*, 9739–9754. [CrossRef] [PubMed]

46. Tezel, E.; Sannes, D.K.; Svelle, S.; Szilágyi, P.Á.; Olsbye, U. Direct CO_2 to methanol reduction on Zr 6-MOF based composite catalysts: A critical review. *Mater. Adv.* **2023**, *4*, 5479–5495. [CrossRef]
47. Sholeha, N.A.; Holilah, H.; Bahruji, H.; Ayub, A.; Widiastuti, N.; Ediati, R.; Jalil, A.A.; Ulfa, M.; Masruchin, N.; Nugraha, R.E. Recent trend of metal promoter role for CO_2 hydrogenation to C1 and C2+ products. *S. Afr. J. Chem. Eng.* **2023**, *44*, 14–30. [CrossRef]
48. Guil-López, R.; Mota, N.; Llorente, J.; Millán, E.; Pawelec, B.; Fierro, J.L.G.; Navarro, R.M. Methanol Synthesis from CO_2: A Review of the Latest Developments in Heterogeneous Catalysis. *Materials* **2019**, *12*, 3902. [CrossRef] [PubMed]
49. Zang, Y.; Liu, T.; Wei, P.; Li, H.; Wang, Q.; Wang, G.; Bao, X. Selective CO_2 Electroreduction to Ethanol over a Carbon-Coated CuOx Catalyst. *Angew. Chem. Int. Ed.* **2022**, *61*, e202209629. [CrossRef] [PubMed]
50. Francke, R.; Schille, B.; Roemelt, M. Homogeneously Catalyzed Electroreduction of Carbon Dioxide—Methods, Mechanisms, and Catalysts. *Chem. Rev.* **2018**, *118*, 4631–4701. [CrossRef] [PubMed]
51. Wu, J.; Huang, Y.; Ye, W.; Li, Y. CO_2 Reduction: From the Electrochemical to Photochemical Approach. *Adv. Sci.* **2017**, *4*, 1700194. [CrossRef] [PubMed]
52. Jiang, X.; Nie, X.; Guo, X.; Song, C.; Chen, J.G. Recent Advances in Carbon Dioxide Hydrogenation to Methanol via Heterogeneous Catalysis. *Chem. Rev.* **2020**, *120*, 7984–8034. [CrossRef] [PubMed]
53. Yang, T.; Mao, X.; Zhang, Y.; Wu, X.; Wang, L.; Chu, M.; Pao, C.-W.; Yang, S.; Xu, Y.; Huang, X. Coordination tailoring of Cu single sites on C3N4 realizes selective CO_2 hydrogenation at low temperature. *Nat. Commun.* **2021**, *12*, 6022. [CrossRef] [PubMed]
54. Kumaravel, V.; Bartlett, J.; Pillai, S.C. Photoelectrochemical conversion of carbon dioxide (CO_2) into fuels and value-added products. *ACS Energy Lett.* **2020**, *5*, 486–519. [CrossRef]
55. Hu, B.; Guild, C.; Suib, S.L. Thermal, electrochemical, and photochemical conversion of CO_2 to fuels and value-added products. *J. CO_2 Util.* **2013**, *1*, 18–27. Correction in *J. CO_2 Util.* **2013**, *2*, 64. [CrossRef]
56. Luo, Y.; Zhang, K.; Li, Y.; Wang, Y. Valorizing carbon dioxide via electrochemical reduction on gas-diffusion electrodes. *InfoMat* **2021**, *3*, 1313–1332. [CrossRef]
57. Liang, F.; Zhang, K.; Zhang, L.; Zhang, Y.; Lei, Y.; Sun, X. Recent development of electrocatalytic CO_2 reduction application to energy conversion. *Small* **2021**, *17*, 2100323. [CrossRef] [PubMed]
58. Liang, S.; Altaf, N.; Huang, L.; Gao, Y.; Wang, Q. Electrolytic cell design for electrochemical CO_2 reduction. *J. CO_2 Util.* **2020**, *35*, 90–105. [CrossRef]
59. Wiranarongkorn, K.; Eamsiri, K.; Chen, Y.; Arpornwichanop, A. A comprehensive review of electrochemical reduction of CO_2 to methanol: Technical and design aspects. *J. CO_2 Util.* **2023**, *71*, 102477. [CrossRef]
60. Palanichamy, V.; Hess, D.M.; Burke, W.M., IV; Frites, M.; Gray, M.L.; Khan, S.U. Reduction of CO_2 to methanol in photoelectrochemical cell: CM-n-TiO_2/Cu. *Electrochem. Soc. Trans.* **2013**, *53*, 47–54. [CrossRef]
61. Linsebigler, A.L.; Lu, G.; Yates, J.T., Jr. Photocatalysis on TiO_2 surfaces: Principles, mechanisms, and selected results. *Chem. Rev.* **1995**, *95*, 735–758. [CrossRef]
62. Kumagai, H.; Tamaki, Y.; Ishitani, O. Photocatalytic systems for CO_2 reduction: Metal-complex photocatalysts and their hybrids with photofunctional solid materials. *Acc. Chem. Res.* **2022**, *55*, 978–990. [CrossRef] [PubMed]
63. Hornberger, L.-S.; Adams, F. Photocatalytic CO_2 conversion using metal-containing coordination polymers and networks: Recent developments in material design and mechanistic details. *Polymers* **2022**, *14*, 2778. [CrossRef] [PubMed]
64. Edelmannova, M.F.; Reli, M.; Nadrah, P.; Rozman, N.; Ricka, R.; Škapin, A.S.; Nosan, M.; Štangar, U.L.; Kočí, K. A comparative study of TiO2 preparation method on their photocatalytic activity for CO_2 reduction. *Catal. Today* **2023**, *413*, 113944. [CrossRef]
65. Ghoussoub, M.; Xia, M.; Duchesne, P.N.; Segal, D.; Ozin, G. Principles of photothermal gas-phase heterogeneous CO_2 catalysis. *Energy Environ. Sci.* **2019**, *12*, 1122–1142. [CrossRef]
66. Meng, X.; Wang, T.; Liu, L.; Ouyang, S.; Li, P.; Hu, H.; Kako, T.; Iwai, H.; Tanaka, A.; Ye, J. Photothermal conversion of CO_2 into CH4 with H_2 over group VIII nanocatalysts: An alternative approach for solar fuel production. *Angew. Chem. Int. Ed.* **2014**, *53*, 11478–11482. [CrossRef] [PubMed]
67. Yu, F.; Wang, C.; Li, Y.; Ma, H.; Wang, R.; Liu, Y.; Suzuki, N.; Terashima, C.; Ohtani, B.; Ochiai, T. Enhanced solar photothermal catalysis over solution plasma activated TiO_2. *Adv. Sci.* **2020**, *7*, 2000204. [CrossRef] [PubMed]
68. Schlögl, R. The role of chemistry in the energy challenge. *ChemSusChem Chem. Sustain. Energy Mater.* **2010**, *3*, 209–222. [CrossRef] [PubMed]
69. Graciani, J.; Mudiyanselage, K.; Xu, F.; Baber, A.E.; Evans, J.; Senanayake, S.D.; Stacchiola, D.J.; Liu, P.; Hrbek, J.; Sanz, J.F. Highly active copper-ceria and copper-ceria-titania catalysts for methanol synthesis from CO_2. *Science* **2014**, *345*, 546–550. [CrossRef] [PubMed]
70. Yang, X.; Kattel, S.; Senanayake, S.D.; Boscoboinik, J.A.; Nie, X.; Graciani, J.; Rodriguez, J.A.; Liu, P.; Stacchiola, D.J.; Chen, J.G. Low pressure CO_2 hydrogenation to methanol over gold nanoparticles activated on a CeO x/TiO_2 interface. *J. Am. Chem. Soc.* **2015**, *137*, 10104–10107. [CrossRef] [PubMed]

71. Kattel, S.; Yan, B.; Yang, Y.; Chen, J.G.; Liu, P. Optimizing binding energies of key intermediates for CO_2 hydrogenation to methanol over oxide-supported copper. *J. Am. Chem. Soc.* **2016**, *138*, 12440–12450. [CrossRef] [PubMed]
72. Kattel, S.; Yu, W.; Yang, X.; Yan, B.; Huang, Y.; Wan, W.; Liu, P.; Chen, J.G. CO_2 hydrogenation over oxide-supported PtCo catalysts: The role of the oxide support in determining the product selectivity. *Angew. Chem. Int. Ed.* **2016**, *55*, 7968–7973. [CrossRef] [PubMed]
73. Zhou, X.; Qu, J.; Xu, F.; Hu, J.; Foord, J.S.; Zeng, Z.; Hong, X.; Tsang, S.C.E. Shape selective plate-form Ga 2 O 3 with strong metal–support interaction to overlying Pd for hydrogenation of CO_2 to CH_3OH. *Chem. Commun.* **2013**, *49*, 1747–1749. [CrossRef] [PubMed]
74. Kostyniuk, A.; Likozar, B. State-of-the-art advancements in the thermocatalytic conversion of CO_2 into ethanol and higher alcohols: Recent progress in catalyst development and reaction mechanisms. *Chem. Eng. J.* **2025**, *503*, 158467. [CrossRef]
75. Low, J.; Yu, J.; Ho, W. Graphene-based photocatalysts for CO_2 reduction to solar fuel. *J. Phys. Chem. Lett.* **2015**, *6*, 4244–4251. [CrossRef] [PubMed]
76. Shinde, G.Y.; Mote, A.S.; Gawande, M.B. Recent advances of photocatalytic hydrogenation of CO_2 to methanol. *Catalysts* **2022**, *12*, 94. [CrossRef]
77. Wang, W.; Wang, S.; Ma, X.; Gong, J. Recent advances in catalytic hydrogenation of carbon dioxide. *Chem. Soc. Rev.* **2011**, *40*, 3703–3727. [CrossRef] [PubMed]
78. Din, I.U.; Shaharun, M.S.; Alotaibi, M.A.; Alharthi, A.I.; Naeem, A. Recent developments on heterogeneous catalytic CO_2 reduction to methanol. *J. CO_2 Util.* **2019**, *34*, 20–33. [CrossRef]
79. Wang, Q.; Astruc, D. State of the art and prospects in metal–organic framework (MOF)-based and MOF-derived nanocatalysis. *Chem. Rev.* **2019**, *120*, 1438–1511. [CrossRef] [PubMed]
80. Zhang, X.; Chen, A.; Zhong, M.; Zhang, Z.; Zhang, X.; Zhou, Z.; Bu, X.-H. Metal–organic frameworks (MOFs) and MOF-derived materials for energy storage and conversion. *Electrochem. Energy Rev.* **2019**, *2*, 29–104. [CrossRef]
81. Li, H.; Eddaoudi, M.; Groy, T.L.; Yaghi, O. Establishing microporosity in open metal− organic frameworks: Gas sorption isotherms for Zn (BDC)(BDC= 1, 4-benzenedicarboxylate). *J. Am. Chem. Soc.* **1998**, *120*, 8571–8572.
82. Li, H.; Eddaoudi, M.; O'Keeffe, M.; Yaghi, O.M. Design and synthesis of an exceptionally stable and highly porous metal-organic framework. *Nature* **1999**, *402*, 276–279. [CrossRef]
83. Rowsell, J.L.C.; Yaghi, O.M. Effects of Functionalization, Catenation, and Variation of the Metal Oxide and Organic Linking Units on the Low-Pressure Hydrogen Adsorption Properties of Metal−Organic Frameworks. *J. Am. Chem. Soc.* **2006**, *128*, 1304–1315. [CrossRef] [PubMed]
84. Horcajada, P.; Serre, C.; Vallet-Regí, M.; Sebban, M.; Taulelle, F.; Férey, G. Metal–Organic Frameworks as Efficient Materials for Drug Delivery. *Angew. Chem.* **2006**, *118*, 6120–6124. [CrossRef]
85. Farha, O.K.; Eryazici, I.; Jeong, N.C.; Hauser, B.G.; Wilmer, C.E.; Sarjeant, A.A.; Snurr, R.Q.; Nguyen, S.T.; Yazaydın, A.Ö.; Hupp, J.T. Metal–Organic Framework Materials with Ultrahigh Surface Areas: Is the Sky the Limit? *J. Am. Chem. Soc.* **2012**, *134*, 15016–15021. [CrossRef] [PubMed]
86. Hönicke, I.M.; Senkovska, I.; Bon, V.; Baburin, I.A.; Bönisch, N.; Raschke, S.; Evans, J.D.; Kaskel, S. Balancing Mechanical Stability and Ultrahigh Porosity in Crystalline Framework Materials. *Angew. Chem. Int. Ed.* **2018**, *57*, 13780–13783. [CrossRef] [PubMed]
87. Moghadam, P.Z.; Li, A.; Wiggin, S.B.; Tao, A.; Maloney, A.G.P.; Wood, P.A.; Ward, S.C.; Fairen-Jimenez, D. Development of a Cambridge Structural Database Subset: A Collection of Metal–Organic Frameworks for Past, Present, and Future. *Chem. Mater.* **2017**, *29*, 2618–2625. [CrossRef]
88. Centi, G.; Čejka, J. Needs and Gaps for Catalysis in Addressing Transitions in Chemistry and Energy from a Sustainability Perspective. *ChemSusChem* **2019**, *12*, 621–632. [CrossRef] [PubMed]
89. Čejka, J.; Nachtigall, P.; Centi, G. New catalytic materials for energy and chemistry in transition. *Chem. Soc. Rev.* **2018**, *47*, 8066–8071. [CrossRef] [PubMed]
90. Centi, G.; Perathoner, S. Creating and mastering nano-objects to design advanced catalytic materials. *Coord. Chem. Rev.* **2011**, *255*, 1480–1498. [CrossRef]
91. Čejka, J.; Centi, G.; Perez-Pariente, J.; Roth, W.J. Zeolite-based materials for novel catalytic applications: Opportunities, perspectives and open problems. *Catal. Today* **2012**, *179*, 2–15. [CrossRef]
92. Eddaoudi, M.; Kim, J.; Rosi, N.; Vodak, D.; Wachter, J.; O'Keeffe, M.; Yaghi, O.M. Systematic design of pore size and functionality in isoreticular MOFs and their application in methane storage. *Science* **2002**, *295*, 469–472. [CrossRef] [PubMed]
93. Kirchon, A.; Feng, L.; Drake, H.F.; Joseph, E.A.; Zhou, H.-C. From fundamentals to applications: A toolbox for robust and multifunctional MOF materials. *Chem. Soc. Rev.* **2018**, *47*, 8611–8638. [CrossRef] [PubMed]
94. Huang, X.; Zhang, S.; Tang, Y.; Zhang, X.; Bai, Y.; Pang, H. Advances in metal–organic framework-based nanozymes and their applications. *Coord. Chem. Rev.* **2021**, *449*, 214216. [CrossRef]
95. Xu, K.; Zhang, S.; Zhuang, X.; Zhang, G.; Tang, Y.; Pang, H. Recent progress of MOF-functionalized nanocomposites: From structure to properties. *Adv. Colloid Interface Sci.* **2024**, *323*, 103050. [CrossRef] [PubMed]

96. Li, D.; Yadav, A.; Zhou, H.; Roy, K.; Thanasekaran, P.; Lee, C. Advances and Applications of Metal-Organic Frameworks (MOFs) in Emerging Technologies: A Comprehensive Review. *Glob. Chall.* **2024**, *8*, 2300244. [CrossRef] [PubMed]
97. Wang, Y.; Yan, J.; Wen, N.; Xiong, H.; Cai, S.; He, Q.; Hu, Y.; Peng, D.; Liu, Z.; Liu, Y. Metal-organic frameworks for stimuli-responsive drug delivery. *Biomaterials* **2020**, *230*, 119619. [CrossRef] [PubMed]
98. Liu, Z.; Chen, Z.; Li, M.; Li, J.; Zhuang, W.; Yang, X.; Wu, S.; Zhang, J. Construction of Single Ni Atom-Immobilized ZIF-8 with Ordered Hierarchical Pore Structures for Selective CO_2 Photoreduction. *ACS Catal.* **2023**, *13*, 6630–6640. [CrossRef]
99. Han, T.-T.; Yang, J.; Liu, Y.-Y.; Ma, J.-F. Rhodamine 6G loaded zeolitic imidazolate framework-8 (ZIF-8) nanocomposites for highly selective luminescent sensing of Fe3+, Cr6+ and aniline. *Microporous Mesoporous Mater.* **2016**, *228*, 275–288. [CrossRef]
100. Xu, C.; Pan, Y.; Wan, G.; Liu, H.; Wang, L.; Zhou, H.; Yu, S.-H.; Jiang, H.-L. Turning on Visible-Light Photocatalytic C−H Oxidation over Metal–Organic Frameworks by Introducing Metal-to-Cluster Charge Transfer. *J. Am. Chem. Soc.* **2019**, *141*, 19110–19117. [CrossRef] [PubMed]
101. Yin, Y.; Hu, B.; Li, X.; Zhou, X.; Hong, X.; Liu, G. Pd@zeolitic imidazolate framework-8 derived PdZn alloy catalysts for efficient hydrogenation of CO_2 to methanol. *Appl. Catal. B Environ.* **2018**, *234*, 143–152. [CrossRef]
102. Hu, B.; Yin, Y.; Zhong, Z.; Wu, D.; Liu, G.; Hong, X. Cu@ZIF-8 derived inverse ZnO/Cu catalyst with sub-5 nm ZnO for efficient CO_2 hydrogenation to methanol. *Catal. Sci. Technol.* **2019**, *9*, 2673–2681. [CrossRef]
103. Chen, F.; Liu, S.; Huang, H.; Wang, B.; Liu, Z.; Jiang, X.; Xiang, W.; Yang, G.; Liu, G.; Peng, X.; et al. Fast synthesis of Cu@zeolitic imidazolate framework-8 (ZIF-8) derived Cu/ZnO catalysts via a facile mechanical grinding method for CO_2 hydrogenation to methanol. *Chem. Sci.* **2025**, *16*, 2273–2286. [CrossRef] [PubMed]
104. Li, X.; Liu, G.; Xu, D.; Hong, X.; Edman Tsang, S.C. Confinement of subnanometric PdZn at a defect enriched ZnO/ZIF-8 interface for efficient and selective CO_2 hydrogenation to methanol. *J. Mater. Chem. A* **2019**, *7*, 23878–23885. [CrossRef]
105. San, X.; Kang, G.; Zhang, L.; Cui, J.; Meng, D.; Qi, J.; Jin, Q. Rich oxygen vacancies in core–shell structured Co3O4-CuO-ZnO@ZIF-8 for boosting CO_2 hydrogenation to methanol. *Adv. Powder Technol.* **2024**, *35*, 104485. [CrossRef]
106. Xie, G.; Bai, X.; Man, Y.; Ren, P.; Jin, R.; Zhang, R.; Ostrikov, K.; Wang, Z.-j.; Yang, Q. High-performance Al-doped Cu/ZnO catalysts for CO_2 hydrogenation to methanol: MIL-53(Al) source-enabled oxygen vacancy engineering and related promoting mechanisms. *Chem. Eng. J.* **2024**, *480*, 148195. [CrossRef]
107. Chen, Y.; Li, H.; Zhao, W.; Zhang, W.; Li, J.; Li, W.; Zheng, X.; Yan, W.; Zhang, W.; Zhu, J.; et al. Optimizing reaction paths for methanol synthesis from CO_2 hydrogenation via metal-ligand cooperativity. *Nat. Commun.* **2019**, *10*, 1885. [CrossRef] [PubMed]
108. Müller, M.; Hermes, S.; Kähler, K.; van den Berg, M.W.E.; Muhler, M.; Fischer, R.A. Loading of MOF-5 with Cu and ZnO Nanoparticles by Gas-Phase Infiltration with Organometallic Precursors: Properties of Cu/ZnO@MOF-5 as Catalyst for Methanol Synthesis. *Chem. Mater.* **2008**, *20*, 4576–4587. [CrossRef]
109. Vali, S.A.; Moral-Vico, J.; Font, X.; Sánchez, A. Cu/ZnO/CeO_2 Supported on MOF-5 as a Novel Catalyst for the CO_2 Hydrogenation to Methanol: A Mechanistic Study on the Effect of CeO_2 and MOF-5 on Active Sites. *Catal. Lett.* **2024**, *154*, 3157–3173. [CrossRef]
110. Zhang, J.; An, B.; Li, Z.; Cao, Y.; Dai, Y.; Wang, W.; Zeng, L.; Lin, W.; Wang, C. Neighboring Zn–Zr Sites in a Metal–Organic Framework for CO_2 Hydrogenation. *J. Am. Chem. Soc.* **2021**, *143*, 8829–8837. [CrossRef] [PubMed]
111. Gutterød, E.S.; Lazzarini, A.; Fjermestad, T.; Kaur, G.; Manzoli, M.; Bordiga, S.; Svelle, S.; Lillerud, K.P.; Skúlason, E.; Øien-Ødegaard, S.; et al. Hydrogenation of CO_2 to Methanol by Pt Nanoparticles Encapsulated in UiO-67: Deciphering the Role of the Metal–Organic Framework. *J. Am. Chem. Soc.* **2020**, *142*, 999–1009. [CrossRef] [PubMed]
112. Treto-Suárez, M.A.; Hidalgo-Rosa, Y.; Saavedra-Torres, M.; Koivisto, B.D.; Mena Ulecia, K.; Páez-Hernández, D.; Zarate, X.; Schott, E. Tunable optical properties of isoreticular UiO-67 MOFs for photocatalysis: A theoretical study. *Dalton Trans.* **2024**, *53*, 11310–11325. [CrossRef] [PubMed]
113. Zhang, C.; Liao, P.; Wang, H.; Sun, J.; Gao, P. Preparation of novel bimetallic CuZn-BTC coordination polymer nanorod for methanol synthesis from CO_2 hydrogenation. *Mater. Chem. Phys.* **2018**, *215*, 211–220. [CrossRef]
114. Fang, Y.; Hong, X.; Chao, D. Photoinduced morphological transformation of a self-assembled iron(ii) coordination polymer: High-performance, non-precious metal, and self-enhancing photocatalytic CO_2 reduction. *Inorg. Chem. Front.* **2024**, *11*, 562–570. [CrossRef]
115. Ling, P.; Lei, J.; Ju, H. Porphyrinic metal-organic framework as electrochemical probe for DNA sensing via triple-helix molecular switch. *Biosens. Bioelectron.* **2015**, *71*, 373–379. [CrossRef] [PubMed]
116. Bao, C.; Huo, Y.-F.; Li, Y.-T.; Yang, S.-Q.; Li, W.; Hu, T.-L. Anchoring Cu on Zirconium-oxo nodes in a pore-confined metal-organic framework for CO_2 hydrogenation to methanol. *Chem. Eng. J.* **2025**, *503*, 158610. [CrossRef]
117. Cavka, J.H.; Jakobsen, S.; Olsbye, U.; Guillou, N.; Lamberti, C.; Bordiga, S.; Lillerud, K.P. A New Zirconium Inorganic Building Brick Forming Metal Organic Frameworks with Exceptional Stability. *J. Am. Chem. Soc.* **2008**, *130*, 13850–13851. [CrossRef] [PubMed]
118. Chui, S.S.-Y.; Lo, S.M.-F.; Charmant, J.P.H.; Orpen, A.G.; Williams, I.D. A Chemically Functionalizable Nanoporous Material $[Cu_3TMA)_2(H_2O)_3]_n$. *Science* **1999**, *283*, 1148–1150. [CrossRef] [PubMed]

119. Yang, S.; Sun, J.; Ramirez-Cuesta, A.J.; Callear, S.K.; David, W.I.F.; Anderson, D.P.; Newby, R.; Blake, A.J.; Parker, J.E.; Tang, C.C.; et al. Selectivity and direct visualization of carbon dioxide and sulfur dioxide in a decorated porous host. *Nat. Chem.* **2012**, *4*, 887–894. [CrossRef] [PubMed]
120. Seo, J.S.; Whang, D.; Lee, H.; Jun, S.I.; Oh, J.; Jeon, Y.J.; Kim, K. A homochiral metal–organic porous material for enantioselective separation and catalysis. *Nature* **2000**, *404*, 982–986. [CrossRef] [PubMed]
121. Grünker, R.; Bon, V.; Müller, P.; Stoeck, U.; Krause, S.; Mueller, U.; Senkovska, I.; Kaskel, S. A new metal–organic framework with ultra-high surface area. *Chem. Commun.* **2014**, *50*, 3450–3452. [CrossRef] [PubMed]
122. Ahnfeldt, T.; Guillou, N.; Gunzelmann, D.; Margiolaki, I.; Loiseau, T.; Férey, G.; Senker, J.; Stock, N. $[Al_4(OH)_2(OCH_3)_4(H_2N\text{-}bdc)_3]\cdot x\,H_2O$: A 12-Connected Porous Metal–Organic Framework with an Unprecedented Aluminum-Containing Brick. *Angew. Chem. Int. Ed.* **2009**, *48*, 5163–5166. [CrossRef] [PubMed]
123. Nadar, S.S.; Vaidya, L.; Maurya, S.; Rathod, V.K. Polysaccharide based metal organic frameworks (polysaccharide–MOF): A review. *Coord. Chem. Rev.* **2019**, *396*, 1–21. [CrossRef]
124. Zulys, A.; Yulia, F.; Muhadzib, N.; Nasruddin. Biological Metal–Organic Frameworks (Bio-MOFs) for CO_2 Capture. *Ind. Eng. Chem. Res.* **2021**, *60*, 37–51. [CrossRef]
125. Sharafi-Badr, P.; Hayati, P.; Mahmoudi, G. Chapter 5—Biological MOFs (bio-MOFs) for energy applications. In *Metal-Organic Framework-Based Nanomaterials for Energy Conversion and Storage*; Gupta, R.K., Nguyen, T.A., Yasin, G., Eds.; Elsevier: Amsterdam, The Netherlands, 2022; pp. 81–103.
126. Leite, J.P.; Figueira, F.v.; Mendes, R.F.; Almeida Paz, F.A.; Gales, L.s. Metal–Organic Frameworks as Sensors for Human Amyloid Diseases. *ACS Sens.* **2023**, *8*, 1033–1053. [CrossRef] [PubMed]
127. Kalmutzki, M.J.; Hanikel, N.; Yaghi, O.M. Secondary building units as the turning point in the development of the reticular chemistry of MOFs. *Sci. Adv.* **2018**, *4*, eaat9180. [CrossRef] [PubMed]
128. Van, N.T.T.; Loc, L.C.; Tri, N.; Cuong, H.T. Synthesis, characterisation, adsorption ability and activity of Cu,ZnO@UiO–66 in methanol synthesis. *Int. J. Nanotechnol.* **2015**, *12*, 405–415. [CrossRef]
129. Rungtaweevoranit, B.; Baek, J.; Araujo, J.R.; Archanjo, B.S.; Choi, K.M.; Yaghi, O.M.; Somorjai, G.A. Copper Nanocrystals Encapsulated in Zr-based Metal–Organic Frameworks for Highly Selective CO_2 Hydrogenation to Methanol. *Nano Lett.* **2016**, *16*, 7645–7649. [CrossRef] [PubMed]
130. Zhao, F.; Fan, L.; Xu, K.; Hua, D.; Zhan, G.; Zhou, S.-F. Hierarchical sheet-like Cu/Zn/Al nanocatalysts derived from LDH/MOF composites for CO_2 hydrogenation to methanol. *J. CO_2 Util.* **2019**, *33*, 222–232. [CrossRef]
131. Zeng, L.; Wang, Y.; Li, Z.; Song, Y.; Zhang, J.; Wang, J.; He, X.; Wang, C.; Lin, W. Highly Dispersed Ni Catalyst on Metal–Organic Framework-Derived Porous Hydrous Zirconia for CO_2 Methanation. *ACS Appl. Mater. Interfaces* **2020**, *12*, 17436–17442. [CrossRef] [PubMed]
132. Pustovarenko, A.; Dikhtiarenko, A.; Bavykina, A.; Gevers, L.; Ramírez, A.; Russkikh, A.; Telalovic, S.; Aguilar, A.; Hazemann, J.-L.; Ould-Chikh, S.; et al. Metal–Organic Framework-Derived Synthesis of Cobalt Indium Catalysts for the Hydrogenation of CO_2 to Methanol. *ACS Catal.* **2020**, *10*, 5064–5076. [CrossRef]
133. Liu, T.; Hong, X.; Liu, G. In situ generation of the Cu@ 3D-ZrO x framework catalyst for selective methanol synthesis from CO_2/H_2. *ACS Catal.* **2020**, *10*, 93–102. [CrossRef]
134. Kobayashi, H.; Taylor, J.M.; Mitsuka, Y.; Ogiwara, N.; Yamamoto, T.; Toriyama, T.; Matsumura, S.; Kitagawa, H. Charge transfer dependence on CO_2 hydrogenation activity to methanol in Cu nanoparticles covered with metal–organic framework systems. *Chem. Sci.* **2019**, *10*, 3289–3294. [CrossRef] [PubMed]
135. Stawowy, M.; Ciesielski, R.; Maniecki, T.; Matus, K.; Łużny, R.; Trawczynski, J.; Silvestre-Albero, J.; Łamacz, A. CO_2 hydrogenation to methanol over ce and zr containing uio-66 and cu/uio-66. *Catalysts* **2020**, *10*, 39. [CrossRef]
136. An, B.; Li, Z.; Song, Y.; Zhang, J.; Zeng, L.; Wang, C.; Lin, W. Cooperative copper centres in a metal–organic framework for selective conversion of CO_2 to ethanol. *Nat. Catal.* **2019**, *2*, 709–717. [CrossRef]
137. Zhang, L.; Cui, J.; Zhang, Y.; San, X.; Meng, D. Surface conversion of CuO–ZnO to ZIF-8 to enhance CO_2 adsorption for CO_2 hydrogenation to methanol. *New J. Chem.* **2023**, *47*, 6700–6707. [CrossRef]
138. Chen, G.; Yu, J.; Li, G.; Zheng, X.; Mao, H.; Mao, D. Cu+-ZrO2 interfacial sites with highly dispersed copper nanoparticles derived from Cu@UiO-67 hybrid for efficient CO_2 hydrogenation to methanol. *Int. J. Hydrog. Energy* **2023**, *48*, 2605–2616. [CrossRef]
139. Cui, W.G.; Zhang, Q.; Zhou, L.; Wei, Z.C.; Yu, L.; Dai, J.J.; Zhang, H.; Hu, T.L. Hybrid MOF Template-Directed Construction of Hollow-Structured In2O3@ZrO2 Heterostructure for Enhancing Hydrogenation of CO_2 to Methanol. *Small* **2023**, *19*, e2204914. [CrossRef] [PubMed]
140. Wang, W.; He, R.; Wang, Y.; Li, M.; Liu, J.; Liang, J.; Yasuda, S.; Liu, Q.; Wu, M.; Tsubaki, N. Boosting Methanol-Mediated CO_2 Hydrogenation into Aromatics by Synergistically Tailoring Oxygen Vacancy and Acid Site Properties of Multifunctional Catalyst. *Chem. A Eur. J.* **2023**, *29*, e202301135. [CrossRef] [PubMed]
141. Han, X.; Li, M.; Chang, X.; Hao, Z.; Chen, J.; Pan, Y.; Kawi, S.; Ma, X. Hollow structured Cu@ZrO2 derived from Zr-MOF for selective hydrogenation of CO_2 to methanol. *J. Energy Chem.* **2022**, *71*, 277–287. [CrossRef]

142. Cai, Z.; Huang, M.; Dai, J.; Zhan, G.; Sun, F.-l.; Zhuang, G.-L.; Wang, Y.; Tian, P.; Chen, B.; Ullah, S.; et al. Fabrication of Pd/In2O3 Nanocatalysts Derived from MIL-68(In) Loaded with Molecular Metalloporphyrin (TCPP(Pd)) Toward CO_2 Hydrogenation to Methanol. *ACS Catal.* **2022**, *12*, 709–723. [CrossRef]
143. Liu, B.; Fang, T.; He, Y. In–Co–Zn/C–N catalysts derived from ZIFs for selective hydrogenation of CO_2 into methanol. *Catal. Sci. Technol.* **2022**, *12*, 300–309. [CrossRef]
144. Qi, T.; Zhao, Y.; Chen, S.; Li, W.; Guo, X.; Zhang, Y.; Song, C. Bimetallic metal organic framework-templated synthesis of a Cu-ZnO/Al2O3 catalyst with superior methanol selectivity for CO_2 hydrogenation. *Mol. Catal.* **2021**, *514*, 111870. [CrossRef]
145. Yang, Y.; Xu, Y.; Ding, H.; Yang, D.; Cheng, E.; Hao, Y.; Wang, H.; Hong, Y.; Su, Y.; Wang, Y.; et al. Cu/ZnOx@UiO-66 synthesized from a double solvent method as an efficient catalyst for CO_2 hydrogenation to methanol. *Catal. Sci. Technol.* **2021**, *11*, 4367–4375. [CrossRef]
146. Zhang, J.; An, B.; Cao, Y.; Li, Z.; Chen, J.; He, X.; Wang, C. ZnO Supported on a Zr-Based Metal–Organic Framework for Selective CO_2 Hydrogenation to Methanol. *ACS Appl. Energy Mater.* **2021**, *4*, 13567–13574. [CrossRef]
147. Ye, J.; Johnson, J.K. Catalytic hydrogenation of CO_2 to methanol in a Lewis pair functionalized MOF. *Catal. Sci. Technol.* **2016**, *6*, 8392–8405. [CrossRef]
148. Wang, C.; Kosari, M.; Xi, S.; Zeng, H.C. Uniform Si-Infused UiO-66 as a Robust Catalyst Host for Efficient CO_2 Hydrogenation to Methanol. *Adv. Funct. Mater.* **2023**, *33*, 2212478. [CrossRef]
149. Yu, J.; Chen, G.; Guo, Q.; Guo, X.; Da Costa, P.; Mao, D. Ultrasmall bimetallic Cu/ZnOx nanoparticles encapsulated in UiO-66 by deposition–precipitation method for CO_2 hydrogenation to methanol. *Fuel* **2022**, *324*, 124694. [CrossRef]
150. Cai, Z.; Dai, J.; Li, W.; Tan, K.B.; Huang, Z.; Zhan, G.; Huang, J.; Li, Q. Pd supported on MIL-68 (In)-derived In2O3 nanotubes as superior catalysts to boost CO_2 hydrogenation to methanol. *ACS Catal.* **2020**, *10*, 13275–13289. [CrossRef]
151. Shi, Y.; Su, W.; Wei, X.; Song, X.; Bai, Y.; Wang, J.; Lv, P.; Yu, G. Highly active MIL-68(In)-derived In2O3 hollow tubes catalysts to boost CO_2 hydrogenation to methanol. *Fuel* **2023**, *334*, 126811. [CrossRef]
152. Koley, P.; Shit, S.C.; Yoshida, T.; Jampaiah, D.; Ariga-Miwa, H.; Uruga, T.; Kaishyop, J.; Hosseinnejad, T.; Periasamy, S.; Gudi, R.D.; et al. Metal organic framework derived In2O3/ZrO2 heterojunctions with interfacial oxygen vacancies for highly selective CO_2-to-methanol hydrogenation. *Nat. Commun.* **2025**, *16*, 8903. [CrossRef] [PubMed]
153. Mitsuka, Y.; Ogiwara, N.; Mukoyoshi, M.; Kitagawa, H.; Yamamoto, T.; Toriyama, T.; Matsumura, S.; Haneda, M.; Kawaguchi, S.; Kubota, Y.; et al. Fabrication of Integrated Copper-Based Nanoparticles/Amorphous Metal–Organic Framework by a Facile Spray-Drying Method: Highly Enhanced CO_2 Hydrogenation Activity for Methanol Synthesis. *Angew. Chem. Int. Ed.* **2021**, *60*, 22283–22288. [CrossRef] [PubMed]
154. Jiang, H.-L.; Liu, B.; Lan, Y.-Q.; Kuratani, K.; Akita, T.; Shioyama, H.; Zong, F.; Xu, Q. From Metal–Organic Framework to Nanoporous Carbon: Toward a Very High Surface Area and Hydrogen Uptake. *J. Am. Chem. Soc.* **2011**, *133*, 11854–11857. [CrossRef] [PubMed]
155. Bavykina, A.; Kolobov, N.; Khan, I.S.; Bau, J.A.; Ramirez, A.; Gascon, J. Metal–organic frameworks in heterogeneous catalysis: Recent progress, new trends, and future perspectives. *Chem. Rev.* **2020**, *120*, 8468–8535. [CrossRef] [PubMed]
156. Howarth, A.J.; Liu, Y.; Li, P.; Li, Z.; Wang, T.C.; Hupp, J.T.; Farha, O.K. Chemical, thermal and mechanical stabilities of metal–organic frameworks. *Nat. Rev. Mater.* **2016**, *1*, 15018. [CrossRef]
157. Bao, S.; Li, J.; Guan, B.; Jia, M.; Terasaki, O.; Yu, J. A green selective water-etching approach to MOF@ mesoporous SiO2 yolk-shell nanoreactors with enhanced catalytic stabilities. *Matter* **2020**, *3*, 498–508. [CrossRef]
158. Zhang, W.; Hu, Y.; Ge, J.; Jiang, H.-L.; Yu, S.-H. A facile and general coating approach to moisture/water-resistant metal–organic frameworks with intact porosity. *J. Am. Chem. Soc.* **2014**, *136*, 16978–16981. [CrossRef] [PubMed]
159. Li, Z.; Zeng, H.C. Armored MOFs: Enforcing soft microporous MOF nanocrystals with hard mesoporous silica. *J. Am. Chem. Soc.* **2014**, *136*, 5631–5639. [CrossRef] [PubMed]
160. Qin, R.; Zeng, H.C. Confined transformation of UiO-66 nanocrystals to yttria-stabilized zirconia with hierarchical pore structures for catalytic applications. *Adv. Funct. Mater.* **2019**, *29*, 1903264. [CrossRef]
161. Khatun, R.; Pal, R.S.; Siddiqui, N.; Kothari, A.C.; Singh, S.; Bal, R. Efficient low-temperature methane conversion to syngas over highly stable nanocrystalline Ni/CeO_2 catalysts using air as an oxidant. *J. Environ. Chem. Eng.* **2026**, *14*, 124746. [CrossRef]
162. Pal, R.S.; Khatun, R.; Kaishyop, J.; Sharma, S.K.; Rana, S.; Singh, S.; Kothari, A.C.; Khan, T.S.; Tripathi, S.; Sarkar, S.; et al. Optimizing Oxygen Vacancies through p-Band Center Modulation of Oxygen in the Li_2WO_4/Mg_6MnO_8 Catalyst for Enhanced Oxidative Coupling of Methane: An Experimental and Theoretical Study. *ACS Catal.* **2025**, *15*, 557–577. [CrossRef]
163. Pal, R.S.; Rana, S.; Sadhu, S.; Khan, T.S.; Poddar, M.K.; Singha, R.K.; Sarkar, S.; Sharma, R.; Bal, R. Highly active and selective Li/MgO catalysts for methane transformation to C2 hydrocarbons: Experimental and DFT study. *Energy Adv.* **2023**, *2*, 180–197. [CrossRef]
164. Samson, K.; Sliwa, M.; Socha, R.P.; Góra-Marek, K.; Mucha, D.; Rutkowska-Zbik, D.; Paul, J.; Ruggiero-Mikołajczyk, M.; Grabowski, R.; Słoczynski, J. Influence of ZrO2 structure and copper electronic state on activity of Cu/ZrO_2 catalysts in methanol synthesis from CO_2. *ACS Catal.* **2014**, *4*, 3730–3741. [CrossRef]

165. Yaghi, O.M.; Li, H. Hydrothermal synthesis of a metal-organic framework containing large rectangular channels. *J. Am. Chem. Soc.* **1995**, *117*, 10401–10402. [CrossRef]
166. Jiang, H.; Alezi, D.; Eddaoudi, M. A reticular chemistry guide for the design of periodic solids. *Nat. Rev. Mater.* **2021**, *6*, 466–487. [CrossRef]
167. Eddaoudi, M.; Moler, D.B.; Li, H.; Chen, B.; Reineke, T.M.; O'keeffe, M.; Yaghi, O.M. Modular chemistry: Secondary building units as a basis for the design of highly porous and robust metal− organic carboxylate frameworks. *Acc. Chem. Res.* **2001**, *34*, 319–330. [CrossRef] [PubMed]
168. Chen, Z.; Kirlikovali, K.O.; Li, P.; Farha, O.K. Reticular chemistry for highly porous metal–organic frameworks: The chemistry and applications. *Acc. Chem. Res.* **2022**, *55*, 579–591. [CrossRef] [PubMed]
169. Schukraft, G.E.; Ayala, S.; Dick, B.L.; Cohen, S.M. Isoreticular expansion of polyMOFs achieves high surface area materials. *Chem. Commun.* **2017**, *53*, 10684–10687. [CrossRef] [PubMed]
170. Velisoju, V.K.; Cerrillo, J.L.; Ahmad, R.; Mohamed, H.O.; Attada, Y.; Cheng, Q.; Yao, X.; Zheng, L.; Shekhah, O.; Telalovic, S. Copper nanoparticles encapsulated in zeolitic imidazolate framework-8 as a stable and selective CO_2 hydrogenation catalyst. *Nat. Commun.* **2024**, *15*, 2045. [CrossRef] [PubMed]
171. Luan, Y.; Qi, Y.; Gao, H.; Zheng, N.; Wang, G. Synthesis of an amino-functionalized metal–organic framework at a nanoscale level for gold nanoparticle deposition and catalysis. *J. Mater. Chem. A* **2014**, *2*, 20588–20596. [CrossRef]
172. Volosskiy, B.; Niwa, K.; Chen, Y.; Zhao, Z.; Weiss, N.O.; Zhong, X.; Ding, M.; Lee, C.; Huang, Y.; Duan, X. Metal-organic framework templated synthesis of ultrathin, well-aligned metallic nanowires. *ACS Nano* **2015**, *9*, 3044–3049. [CrossRef] [PubMed]
173. Brix, F.; Desbuis, V.; Piccolo, L.; Gaudry, É. Tuning adsorption energies and reaction pathways by alloying: PdZn versus Pd for CO_2 hydrogenation to methanol. *J. Phys. Chem. Lett.* **2020**, *11*, 7672–7678. [CrossRef] [PubMed]
174. Navarro-Jaén, S.; Virginie, M.; Bonin, J.; Robert, M.; Wojcieszak, R.; Khodakov, A.Y. Highlights and challenges in the selective reduction of carbon dioxide to methanol. *Nat. Rev. Chem.* **2021**, *5*, 564–579. [CrossRef] [PubMed]
175. Zhong, J.; Yang, X.; Wu, Z.; Liang, B.; Huang, Y.; Zhang, T. State of the art and perspectives in heterogeneous catalysis of CO_2 hydrogenation to methanol. *Chem. Soc. Rev.* **2020**, *49*, 1385–1413. [CrossRef] [PubMed]
176. Wang, Y.; Winter, L.R.; Chen, J.G.; Yan, B. CO_2 hydrogenation over heterogeneous catalysts at atmospheric pressure: From electronic properties to product selectivity. *Green Chem.* **2021**, *23*, 249–267. [CrossRef]
177. Kattel, S.; Yan, B.; Chen, J.G.; Liu, P. CO_2 hydrogenation on Pt, Pt/SiO2 and Pt/TiO2: Importance of synergy between Pt and oxide support. *J. Catal.* **2016**, *343*, 115–126. [CrossRef]
178. Chen, W.; Cao, J.; Fu, W.; Zhang, J.; Qian, G.; Yang, J.; Chen, D.; Zhou, X.; Yuan, W.; Duan, X. Molecular-level insights into the notorious CO poisoning of platinum catalyst. *Angew. Chem. Int. Ed.* **2022**, *61*, e202200190. [CrossRef] [PubMed]
179. Noh, G.; Lam, E.; Bregante, D.T.; Meyet, J.; Šot, P.; Flaherty, D.W.; Copéret, C. Lewis Acid Strength of Interfacial Metal Sites Drives CH3OH Selectivity and Formation Rates on Cu-Based CO_2 Hydrogenation Catalysts. *Angew. Chem.* **2021**, *133*, 9736–9745. [CrossRef]
180. Tedeeva, M.A.; Kustov, A.L.; Batkin, A.M.; Garifullina, C.; Zalyatdinov, A.A.; Yang, D.; Dai, Y.; Yang, Y.; Kustov, L.M. Catalytic systems for hydrogenation of CO_2 to methanol. *Mol. Catal.* **2024**, *566*, 114403. [CrossRef]
181. Lu, X.; Song, C.; Qi, X.; Li, D.; Lin, L. Confinement Effects in Well-Defined Metal–Organic Frameworks (MOFs) for Selective CO_2 Hydrogenation: A Review. *Int. J. Mol. Sci.* **2023**, *24*, 4228. [CrossRef] [PubMed]
182. Li, Y.-M.; Hu, J.; Zhu, M. Confining atomically precise nanoclusters in metal–organic frameworks for advanced catalysis. *Coord. Chem. Rev.* **2023**, *495*, 215364. [CrossRef]
183. Gutterød, E.S.; Pulumati, S.H.; Kaur, G.; Lazzarini, A.; Solemsli, B.G.; Gunnæs, A.E.; Ahoba-Sam, C.; Kalyva, M.E.; Sannes, J.A.; Svelle, S.; et al. Influence of Defects and H2O on the Hydrogenation of CO_2 to Methanol over Pt Nanoparticles in UiO-67 Metal–Organic Framework. *J. Am. Chem. Soc.* **2020**, *142*, 17105–17118. [CrossRef] [PubMed]
184. Hu, J.; Yu, L.; Deng, J.; Wang, Y.; Cheng, K.; Ma, C.; Zhang, Q.; Wen, W.; Yu, S.; Pan, Y.; et al. Sulfur vacancy-rich MoS2 as a catalyst for the hydrogenation of CO_2 to methanol. *Nat. Catal.* **2021**, *4*, 242–250. [CrossRef]
185. Dhakshinamoorthy, A.; Opanasenko, M.; Čejka, J.; Garcia, H. Metal organic frameworks as heterogeneous catalysts for the production of fine chemicals. *Catal. Sci. Technol.* **2013**, *3*, 2509–2540. [CrossRef]
186. Yaghi, O.M.; O'Keeffe, M.; Ockwig, N.W.; Chae, H.K.; Eddaoudi, M.; Kim, J. Reticular synthesis and the design of new materials. *Nature* **2003**, *423*, 705–714. [CrossRef] [PubMed]
187. Centi, G.; Iaquaniello, G.; Perathoner, S. Chemical engineering role in the use of renewable energy and alternative carbon sources in chemical production. *BMC Chem. Eng.* **2019**, *1*, 5. [CrossRef]
188. Centi, G.; Perathoner, S. Chemistry and energy beyond fossil fuels. A perspective view on the role of syngas from waste sources. *Catal. Today* **2020**, *342*, 4–12. [CrossRef]
189. Yarulina, I.; Chowdhury, A.D.; Meirer, F.; Weckhuysen, B.M.; Gascon, J. Recent trends and fundamental insights in the methanol-to-hydrocarbons process. *Nat. Catal.* **2018**, *1*, 398–411. [CrossRef]

190. Ronda-Lloret, M.; Rothenberg, G.; Shiju, N.R. A critical look at direct catalytic hydrogenation of carbon dioxide to olefins. *ChemSusChem* **2019**, *12*, 3896–3914. [CrossRef] [PubMed]
191. Tian, P.; Wei, Y.; Ye, M.; Liu, Z. Methanol to olefins (MTO): From fundamentals to commercialization. *Acs Catal.* **2015**, *5*, 1922–1938. [CrossRef]
192. Yang, M.; Fan, D.; Wei, Y.; Tian, P.; Liu, Z. Recent progress in methanol-to-olefins (MTO) catalysts. *Adv. Mater.* **2019**, *31*, 1902181. [CrossRef] [PubMed]
193. Olsbye, U.; Bjørgen, M.; Svelle, S.; Lillerud, K.-P.; Kolboe, S. Mechanistic insight into the methanol-to-hydrocarbons reaction. *Catal. Today* **2005**, *106*, 108–111. [CrossRef]
194. Rubio-Martinez, M.; Avci-Camur, C.; Thornton, A.W.; Imaz, I.; Maspoch, D.; Hill, M.R. New synthetic routes towards MOF production at scale. *Chem. Soc. Rev.* **2017**, *46*, 3453–3480. [CrossRef] [PubMed]

Disclaimer/Publisher's Note: The statements, opinions and data contained in all publications are solely those of the individual author(s) and contributor(s) and not of MDPI and/or the editor(s). MDPI and/or the editor(s) disclaim responsibility for any injury to people or property resulting from any ideas, methods, instructions or products referred to in the content.